AD 274 113

638 300

MASSACHUSETTS INSTITUTE OF TECHNOLOGY
NAVAL SUPERSONIC LABORATORY

TECHNICAL REPORT 465

A STUDY OF SATELLITE DECAY WITH THE FIRST AND SECOND ORDER GRAVITATIONAL POTENTIAL

by

R. E. Good

June 1961

MASSACHUSETTS INSTITUTE OF TECHNOLOGY
Naval Supersonic Laboratory

TECHNICAL REPORT 465

A STUDY OF SATELLITE DECAY WITH THE FIRST AND SECOND ORDER GRAVITATIONAL POTENTIAL

by

R. E. Good

M. I. T. DSR 8304
Contract AF19(604)-5894

June 1961

FOREWORD

The work reported herein was sponsored by the Air Force Systems Command under Contract AF19(604)-5894. Dr. G. R. Miczaika and Dr. H. B. Wackernagel monitored the program for the Air Force.

ABSTRACT

The decay of earth satellites has been analyzed using both a numerical integration and an approximate method. The numerical integration utilizes the variation-of-parameter method with second order earth gravitational potential. The approximate method was developed via conservation of energy equation but for unexplained reasons would not agree with observed satellite decay without the inclusion of an additional linear eccentricity factor. Including $(c/100)^{0.366}$ permitted the approximate method to agree with numerical calculations and observed data. The usual restriction of approximate methods at low eccentricities was removed by the addition of a non-linear term previously computed numerically. The linear approximate method was found to be valid for linear eccentricities larger than 150. The effect of a variable drag coefficient and projected area was found to be an important factor and of the order e^2.

TABLE OF CONTENTS

LIST OF ILLUSTRATIONS

LIST OF ILLUSTRATIONS - (Continued)

LIST OF TABLES

LIST OF SYMBOLS

A	Satellite angle of attack
a	Semi-major axis
B	Satellite angle of yaw
B_1	Magnetic field strength
C	Satellite angle of roll
C_D	Drag coefficient
$\left(\frac{C_D A}{m}\right)$	Ballistic coefficient, cm^2/Kg
$\left(\frac{C_D A}{w}\right)$	Ballistic coefficient, ft^2/lb
c	Linear eccentricity
D	Jeffrey's coefficient for the third order gravitational term
E_D	Energy due to drag force
E or e	Eccentricity
F	Perturbing force
f	True anomaly
G	Density scale height
g	Local gravity
H	Pressure scale height
H_γ	Momentum vector
h	Altitude
I_0	Modified Bessel function of zero order
I_1	Modified Bessel function of first order
J	Jeffrey's coefficient for the second order gravitational term
j	Current
KM	Earth's gravitational constant
K_n	Knudsen number
L_m	dT_M/dH
M	Air mass
m	Satellite mass
N	Revolution
N_s	Total number of revolutions in spiral decay

P	Orbit parameter
P_N	Legendre polynomial
P_f	Anomalistic period
Q	Apogee distance from earth's center
q	Perigee distance from earth's center
$R_\oplus$	Earth's equatorial radius
$\mathcal{R}$	Accommodation coefficient
R	Universal gas constant
r	Radius
S	Molecular speed ratio
T	Air temperature
T_M	Molecular temperature
T_{skin}	Satellite surface temperature
U	Gravitation potential
V	Satellite velocity
V_{c_r}	Satellite velocity in circular orbit
V_q	Satellite velocity at perigee
v	Most probable molecular velocity
v_r	Molecular re-emission velocity
α	Orbit inclination
ζ	Prolate ellipsoid coordinate
η	Prolate ellipsoid coordinate
θ	Angle between current and magnetic lines
λ	Longitude
ρ	Atmospheric density
ϕ	Polar angle
ψ	Latitude
Ω	Angular velocity
ω	Argument of perigee
Ω_o	Argument of right ascension
Υ	Vernal equinox (Ram's horns or the first point of Aries)

Subscripts

0	Reference altitude
b	Base of a constant L_m
s	Specular reflection
d	Diffuse reflection
T	Total
ϕ	Represent vector direction
α	
E	
N	
Ω_o	
γ	
ω	

I. INTRODUCTION

The motion of satellites is no longer a new subject. The flood of papers and notes in current journals would indicate that considerable attention has been given to the problems of space flight and atmospheric re-entry. In many of these studies the analysis pertains to one of two aspects: orbital motion or re-entry. Less attention has been given to discussion of the satellite's motion throughout its entire lifetime. In particular, analysis of the transition flight between orbit and re-entry has been lacking. This study has been a two-pronged analysis of satellite motion with the object being decay prediction. The analysis is two-pronged in that both an approximate method which permits graphical or similarly equally easy solutions and refined methods requiring numerical integration by modern computing machines are employed.

The approximate method reviewed and improved by an empirical factor, is limited in long range prediction by the nature of the sun's influence upon the earth's atmosphere. This is important, however, only above 300 km. The form of the solutions obtained through the approximate method is well suited for analysis of the gross satellite motion, decay, and atmospheric density. More detailed information is to be gathered from the numerical solutions of the general three-dimensional equations. The three-dimensional equations of motion equate the satellite acceleration to the perturbing function. The perturbing function is made up of the first and second orders of the earth's gravitational potential, and lift and drag forces. The orientation of the satellite in space is also noted. The second order differential equations are reduced to six first order differential equations using the well known variation-of-parameter technique. The solution of these six equations simultaneously is obtained numerically with an IBM 709. The variation-of-parameter perturbation technique is well suited for describing the satellite motion throughout the transition flight but is limited to the order of several hundred revolutions by machine time. Since this is a numerical solution, the analysis of satellite motion consists in observations of several cases. This calculation describes the secular and periodic motion of the orbital elements.

The numerical solution also serves as an "exact" solution to check the approximate method. Also the approximate method is corrected to agree with the numerical solution.

II. FORCES ACTING ON AN EARTH SATELLITE

A satellite launched into an orbit about the earth travels through a magnetic field, a radiation field, and the earth's atmosphere. These fields can cause either a retarding or an accelerating force. The most important force is the drag and lift created as the satellite passes through the earth's dense atmosphere. Each of these forces will be examined in detail in this section. Four fundamental satellite shapes will be considered; sphere, flat plate, cylinder, and prolate ellipsoid. Most any actual satellite can be thought as a composite of one or more of these shapes. The final outcome of this section is the writing of the perturbing function.

A. Forces due to the presence of celestial bodies

1. The earth

The gravitational potential of the earth can be expressed as an infinite series

$$U = -\frac{KM}{r}\left[1 - \sum_{n=1}^{\infty} J_n \left(\frac{R_\oplus}{r}\right)^n P_n(\sin\psi)\right] \qquad (2.1)$$

where ψ represents the latitude and $R_\oplus$ the earth's equatorial radius. The equatorial radius is given as 6378.145 km. The earth's gravitational constant, KM, is equal to 3.98614×10^5 km^3/sec^2. The coefficients of the series were originally designated by Jeffrey (1) as J and D, where

$$J_2 = \frac{2}{3} J$$

$$J_4 = -\frac{8}{35} D$$

The J and D coefficients have been redetermined since that time by Cornford, King-Hele, and Merson (Ref. 2) through observations of the secular satellite orbit motions. The current values are

$$J = [1624.6 \pm 0.3] \times 10^{-6}$$

$$D = [5.7 \pm 0.8] \times 10^{-6}$$

Before the secular motions of the earth satellite were available for study, the odd harmonic terms of the series for the earth's gravitational potential were assumed to be zero, i.e., the earth was thought to be symmetric about the equator. Now it has been shown that the odd harmonics do exist. The first harmonic can, however, be made zero by placing the axis system at the center of mass. When the center of mass is not at the point of symmetry, other difficulties will be encountered in determining the height from the earth's surface and the corresponding density.

The force per unit mass acting on the satellite due to the earth's gravitational potential is the potential gradient $F = -\nabla U$. With spherical polar coordinates centered at the center of mass, the components of the gravitational force along the radius, latitude and longitude, respectively, are

$$\frac{F_r}{m} = -\frac{\partial U}{\partial r} = -\frac{KM}{r^2}\left[1 + J\left(\frac{R}{r}\right)^2 (1 - 3\sin^2\psi) - \frac{D}{7}\left(\frac{R}{r}\right)^4 (35\sin^4\psi - 30\sin^2\psi + 3) + \cdots\right] \tag{2.2}$$

$$\frac{F_\psi}{m} = -\frac{1}{r}\frac{\partial U}{\partial \psi} = J\,KM\left(\frac{R^2}{r^4}\right)\sin 2\psi + \frac{2D}{7}\,KM\left(\frac{R^4}{r^6}\right)\sin 2\psi\,(3 - 7\sin^2\psi) + \cdots$$

$$\frac{F_\lambda}{m} = -\frac{1}{r \sin\psi} \frac{\partial U}{\partial \lambda} = 0$$

It is usually more convenient to use a coordinate system located in the orbit plane rather than the geocentric system above. The axis system in the orbital plane is designated r, ϕ, α (see Figure 1). The direction of ϕ is in the plane perpendicular to the radius vector and α is the direction normal to the orbital plane. Several relations between the two axis systems will be useful. These can be found through the use of spherical and plane trigonometry.

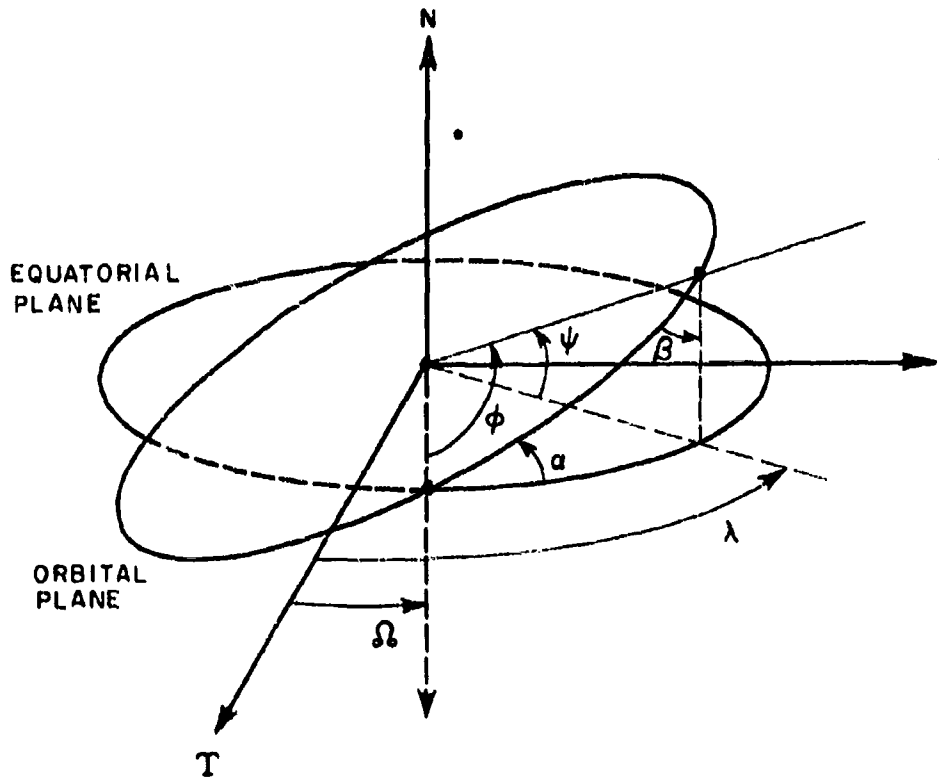

Figure 1. Relations between geocentric and orbit axis system

These relations are

$$(1)\ \cos\phi = \cos(\lambda - \Omega)\cos\psi$$

$$(2)\ \sin\psi = \sin\phi\ \sin\alpha$$

$$(3)\ \cos\alpha = \cos\psi\ \sin\beta$$

$$(4)\ \sin\beta = \frac{\sin(\lambda - \Omega)}{\sin\phi}$$

$$(5)\ \tan\alpha = \frac{\tan\psi}{\sin(\lambda - \Omega)}$$

With the axis system located in the orbital plane, the components of force due to the earth's gravitational potential are

$$\frac{F_r}{m} = -\frac{KM}{r^2}\left[1 + J\left(\frac{R}{r}\right)^2(1 - 3\sin^2\phi\ \sin^2\alpha) - \frac{D}{7}\left(\frac{R}{r}\right)^4(35\ \sin^4\phi\ \sin^4\alpha - 30\sin^2\phi\ \sin^2\alpha + 3) + \cdots\right]$$

$$\frac{F_\phi}{m} = 2J\,KM\,\frac{R^2}{r^4}\sin^2\alpha\ \sin\phi\cos\phi + \frac{D}{7}\,\frac{R^4}{r^6}\,KM\left[28\sin^4\alpha\ \sin^3\phi\ \cos\phi - 12\sin^2\alpha\ \sin\phi\cos\phi\right] \qquad (2.3)$$

$$\frac{F_\alpha}{m} = 2J\,KM\,\frac{R^2}{r^4}\ \sin\phi\ \sin\alpha\cos\alpha + \frac{D}{7}\,\frac{R^4}{r^6}\,KM\left[28\ \sin^3\phi\ \sin^3\alpha\cos\alpha - 12\sin\phi\ \sin\alpha\cos\alpha\right]$$

In addition to the forces due to the earth's gravitational potential, there is a force due to the interaction between the satellite and the earth's magnetic field. This force was, for example, predominant in causing the motion of the Tiros I spin vector (Ref. 3). Previously (Ref. 4), the only interaction considered was due to the cutting of the earth's magnetic lines by the induced electrical charge. Another interaction which should be included is between the satellite internal current and the earth's magnetic field. Such a force is described by

$$F = j \times B_1$$

In particular

$$dF = 0.10\, i(dS \times B_1) \quad \text{dynes}$$

where the current (amperes), i, flows in a length (centimeters) dS of wire in a magnetic field (Gauss)B. For Tiros I, there is an equivalent current of one ampere flowing around the eight-foot base diameter which produces a force of

$$F = 23 \sin\theta \quad \text{dynes}$$

where θ is the angle between the current and the magnetic lines. This force is comparable to the drag force. The force is, however, not always of the same sign. The existence of this force resulting from an internal current is extremely important and bears further examination.

2. The Sun and Moon

The sun exerts considerable influence upon a satellite, either by gravity, radiation pressure, or indirectly through its influence upon the earth's atmosphere. The nature of these influences has been discussed in detail by many authors. The conclusions to date are that atmospheric heating is the means of increasing the density during exposure to the sun. Another observed phenomenon associates an increased drag with solar storms. This latter correlation has lessened the hope of developing long range decay prediction since solar storms are as yet un-

predictable. The obvious escape from this difficulty is to limit the analysis to altitudes below 300 km where the sun's influence has been observed to be small or non-existent. Other difficulties are encountered also above 300 km. At extreme ranges, of the order of the earth's radii or more, the solar gravity field and radiation pressure, as well as the lunar gravitational field, must be included in the perturbing function.

The sun and moon have an influence on the earth's atmosphere below 200 km in the form of atmospheric tides. Atmospheric tides have been detected from pressure measurements to occur twice a day and have an amplitude of 2 mm Hg pressure change. This is equivalent to a 2 km altitude change. Observations of satellites, have not as yet, revealed a behavior which can be attributed to atmospheric tides. It is unlikely that a variation of 2 km would be important in view of the present state of knowledge of the varying ionospheric density.

B. Forces due to the presence of the earth's atmosphere

The satellite passing through the earth's atmosphere experiences aerodynamic forces of lift and drag as well as moments about the center of gravity. These aerodynamic forces and moments can seriously effect the satellite orbit. The effect of drag is well known but whether lift and moments augment or diminish the decay is not so well understood. An analysis of the effects of these three quantities on the lifetime of a satellite is presented in this section. First, however, the earth's atmosphere should be specified.

In free molecular flow, the number and energy state of the air particles is of interest. Usually, the density is expressed functionally as an exponential

$$\rho = \rho_0 \exp\left[-\frac{(h - h_0)}{H}\right] \tag{2.5}$$

where H represents the scale height defined as

$$H = \frac{R_0 T}{gM} = \frac{R_0 T_M}{gM_0} \qquad (2.6)$$

As can be seen, the scale height is a function of the atmospheric temperature and molecular mass. Consequently, Equation (2.5) is limited to an altitude close to the reference altitude (h_0). Above 300 km, the variation of the scale height and density are nearly linear and Equation (2.5) is valid over a range of 100 km above the reference altitude. As an example, starting at 300 km, the density using Equation (2.5) will be 20 per cent too low at 360 km. The error is much larger if the reference altitude is between 100 and 300 km. This is to be expected since the region between 100 and 300 km is the transition between two functions which fit the atmospheric data. As a further example, for a reference altitude at 200 km, the error at 260 km is about 50 per cent too low.

An alternate expression which more closely fits observed values above 350 km is a power function,

$$\rho = \rho_0 \left(\frac{h_0}{h} \right)^n \qquad (2.7)$$

The value of n which fits the 1959 ARDC model atmosphere is about 1/6. A smoother representation would result if the value of 6.38 is used. Figure 2 is a comparison of this function with the atmospheric model.

In place of either of these two equations, the actual atmospheric model can be used. In machine computations such as used for this study, a subroutine to look up and interpolate the atmospheric table can be incorporated. This form is necessary in attempting to preserve accuracy throughout the computations.

Each of these three methods inherently assumes that the earth's atmosphere has the same shape as the earth. Logically, it would be expected that the oblateness of the atmosphere would be different from the oblateness of the earth. A more exact shape is currently being evaluated by Jacchia (Ref. 5).

In addition to the density, a model of the atmospheric temperature and mass is required. These two quantities are sometimes grouped

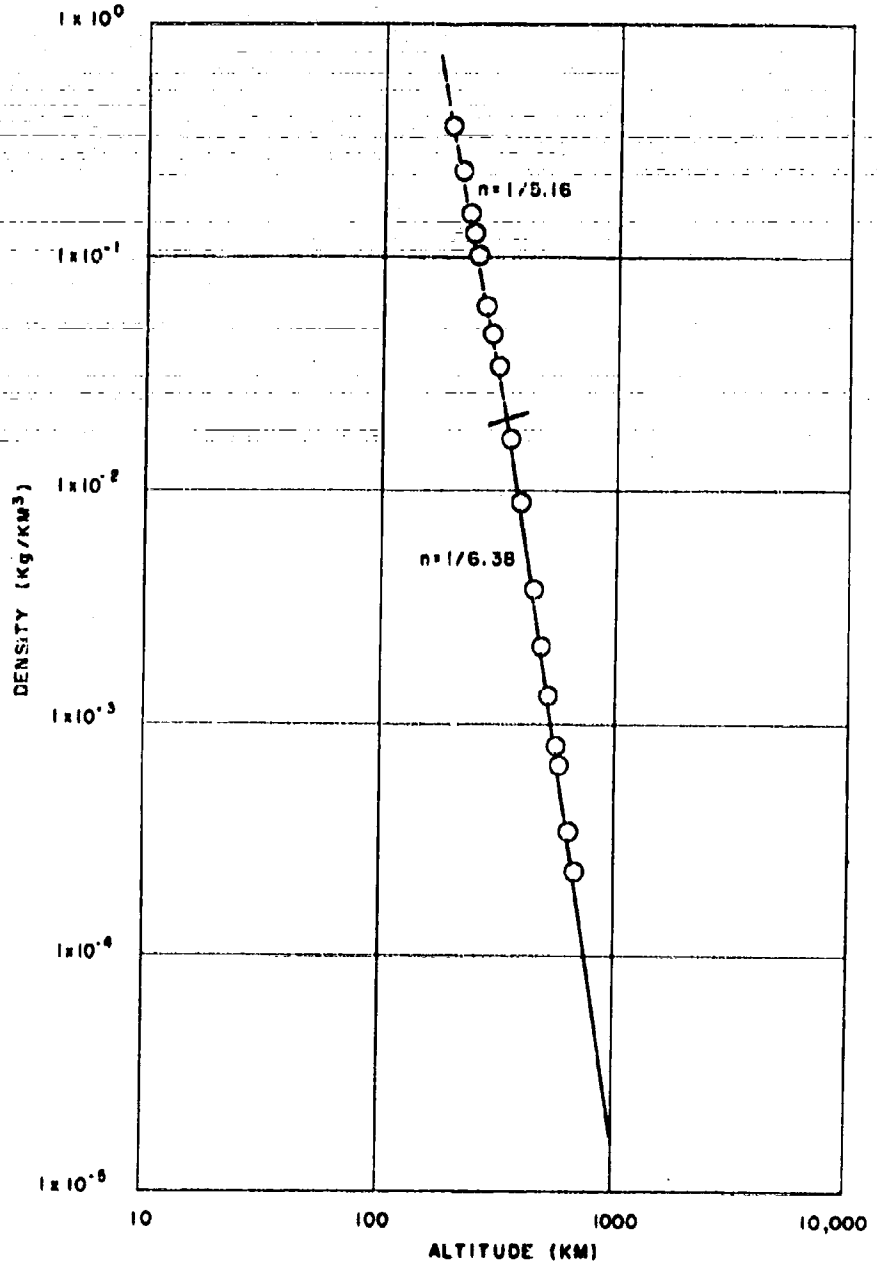

Figure 2. Atmospheric Density

together as the molecular-scale temperature. The following is the general form of the molecular-scale temperature function (Ref. 6).

$$T_M = (T_M)_b + L_M(H - H_b) \tag{2.8}$$

where

H = Geopotential altitude in km

T_M = The molecular-scale temperature is °K at altitude H

$L_M = dT_M/dH$

H_b = Geopotential in km at the base of a particular layer characterized by a specific value of L_M

$(T_M)_b$ = The value of T_M at altitude H_b

The values of the coefficients are given in Table 1.

Table 1

Temperature-Height Profile of 1959 ARDC Model Atmosphere

H_b	$(T_M)_b$	L_M ~ °K/km
79	165.66	0.0
90	165.66	4.0
105	225.66	2.0
160	1325.66	1.0
170	1425.66	0.5
200	1575.66	0.35
700	3325.66	0.35

1. Drag forces

The drag force acting on the satellite is proportional to the dynamic pressure and the area. The factor of proportionality, termed the drag coefficient, is a function of the relative velocity of the satellite with respect to the atmosphere, the density of the atmosphere, and the surface conditions of the satellite. The density of the atmosphere dictates which aerodynamic approximation is used to describe the drag coefficient. The

regions of flow to which each approximation is applicable are commonly separated by the Knudsen number, a non-dimensional ratio of the mean free path to some pertinent body dimension. Experiments in free molecular flow (Ref. 7) indicate that the "so-called" free molecular theory becomes applicable when the Knudsen number is greater than two. As discussed previously (Ref. 4), free molecular theory is, on this basis, valid for all satellite orbits above 130 km (assuming a satellite length of 25 m). The launching of larger satellites such as the 100-foot balloon, will require the addition of a transition drag correction to the free molecular flow theory as the satellites descend below 160 km. The dependence of the drag coefficient on the satellite velocity and surface condition will not be derived from first principles in the succeeding sections. For a more detailed discussion of the drag coefficient, the reader is referred to Refs. 8, 9, and 10.

(a) Estimation of molecular speed ratio

One of the basic dimensionless parameters in the free molecular flow is called the molecular speed ratio, and is defined as:

$$S = \frac{V}{v}$$

where

$$v = \sqrt{2RT_M}$$

The satellite velocity is denoted as V and the most probable molecular speed as v. The molecular-scale temperature, and the gas constant R are obtained from Ref. 6.

A range for possible molecular speed ratios encountered by satellites at various altitudes is of interest. The minimum molecular speed ratio will be defined in terms of Vc_r,

$$S_{min} = \frac{Vc_r}{v}$$

where Vc_r is the circular satellite velocity at a distance r from the earth's center and is defined as

$$Vc_r = \sqrt{\frac{KM}{r}}$$

For vehicles in elliptical orbits, the total velocity is given as

$$V = \sqrt{\frac{KM}{r}} \frac{(1 + 2e\cos f + e^2)^{1/2}}{1 + e\cos f} \qquad (2.9)$$

The earth's gravitational constant is represented as KM. The velocity at perigee can be expressed as a function of the circular velocity by

$$V_q = Vc_r(1 + e) \qquad (2.10)$$

It can be seen that the velocity at perigee for an elliptical orbit of low eccentricity (such as most satellites around the earth) is only slightly larger than the circular satellite velocity at the same point, and that the minimum speed ratio is a good representation of the actual molecular speed ratio at the perigee points.

The molecular velocity as a function of altitude is illustrated by Figure 3 while the values of S_{min} as functions of altitude are plotted in Figure 4. It is seen that in the 150-600 km altitude range, the range of interest for present earth satellites, the minimum molecular speed ratio ranges between six and ten. The most probable molecular speed increases from a value of 0.782 km/sec at 150 km to 1.285 km/sec at 600 km.

For conditions of diffuse reflection, the drag coefficient will be based on the re-emission speed ratio, S_r. The velocity of re-emission is not clearly defined. Most likely it is a function of the surface conditions. However, the only readily available measure of conditions is the surface temperature. Consequently, it is usual to assume the velocity of re-emission to be

$$V_r = \sqrt{2RT_{skin}}$$

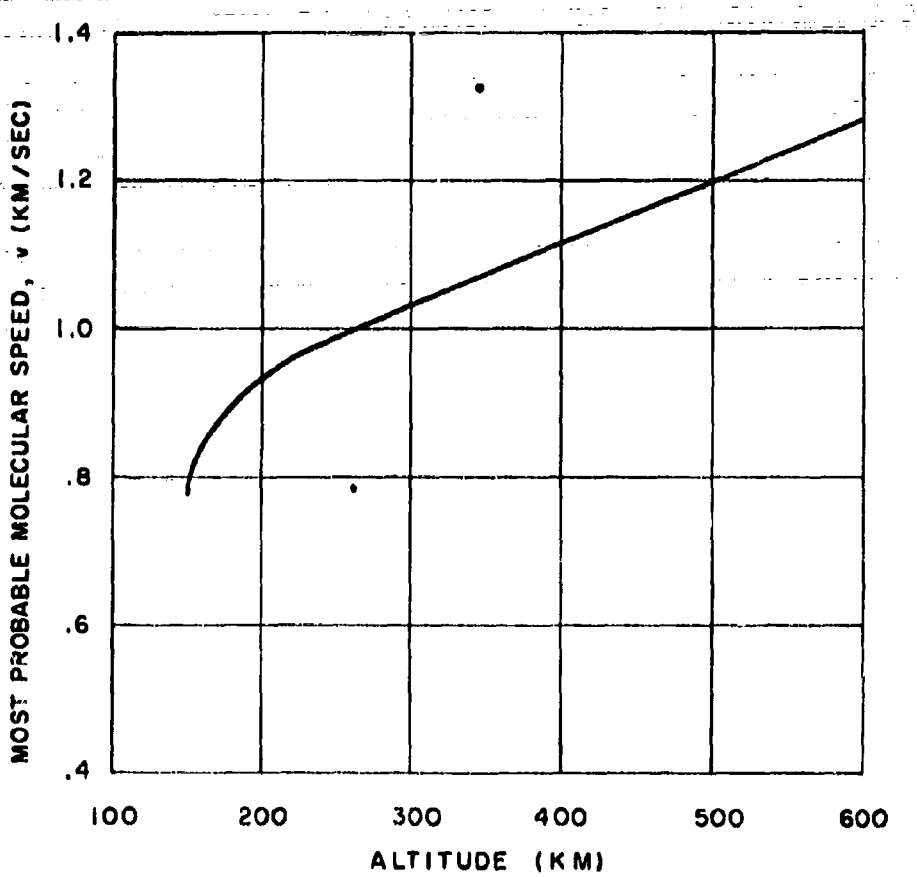

Figure 3. Most probable molecular speed as a function of altitude

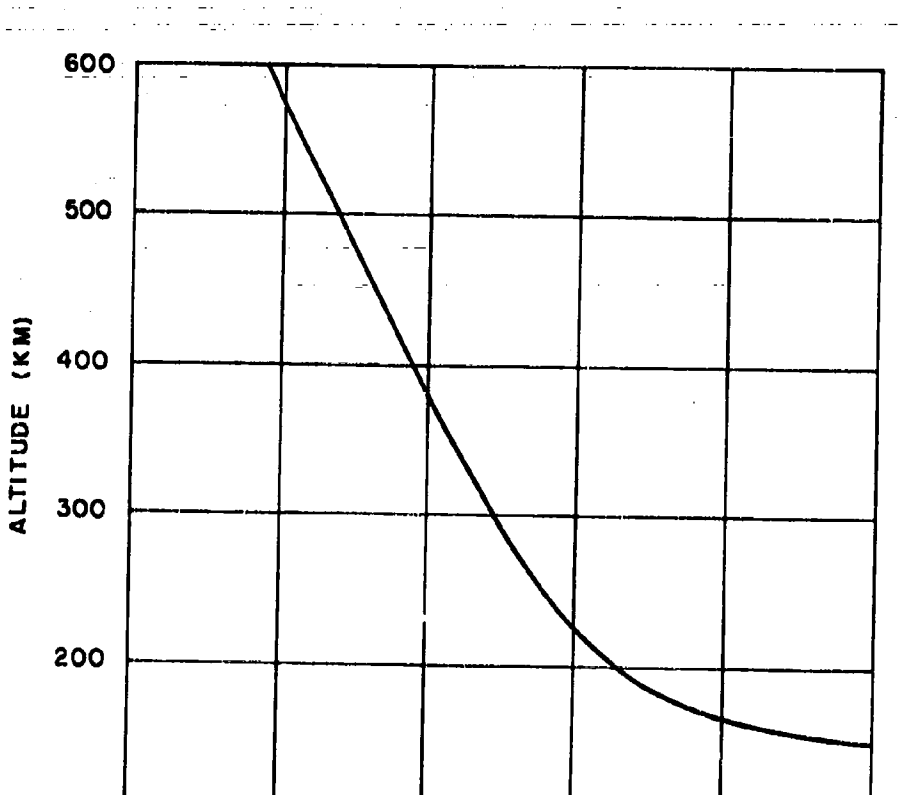

Figure 4. Minimum molecular speed ratio as a function of altitude

The wall temperature varies from recovery temperature to ambient gas temperature. Above an altitude of about 200 km the heat transfer due to the incident molecules becomes less than the solar flux. Consequently, the wall temperature is determined from a radiation balance. Since it is unlikely that the emissivity of the satellite can be made less than 0.01, the maximum surface temperature above 200 km will be 1250 °K. This temperature will always be less than the free-stream temperature above 200 km in which case the re-emission speed ratio can be specified as equal to the incident molecular speed ratio.

For flight below 200 km where free molecular heat transfer is important, the re-emission speed ratio can be computed (Ref. 7) for the extreme case of no heat transfer. This neglects effects of radiation and conduction. Stalder obtained experimental verification for this condition using a Knudsen number of two. The functional relation between the two speed ratios can be approximated as

$$S_r = 1.645 - 0.18(6 - S)^2 \quad ; \quad S < 6 \qquad (2.11)$$

This is to say, the re-emission speed ratio is always much smaller than the incident molecular speed ratio (see Figure 5). The effects of conduction and radiation are expected to drastically reduce the surface temperature and thereby increase the re-emission speed ratio. If recovery temperature was reached or in effect, radiation and conduction were negligible, the drag due to the re-emission could contribute a maximum of 40 per cent of the total drag force as will be seen shortly. In practice this will not occur but it is interesting to note that the drag coefficient could become atmospheric dependent through a variation of the re-emission speed ratio.

(b) Estimation of drag coefficient

Initially the satellite will be in free molecular flow which is assumed to exist when the atmospheric mean free path is equal to twice the characteristic dimension of the satellite. Experiments have been made which verify this assumption. When the Knudsen number becomes less

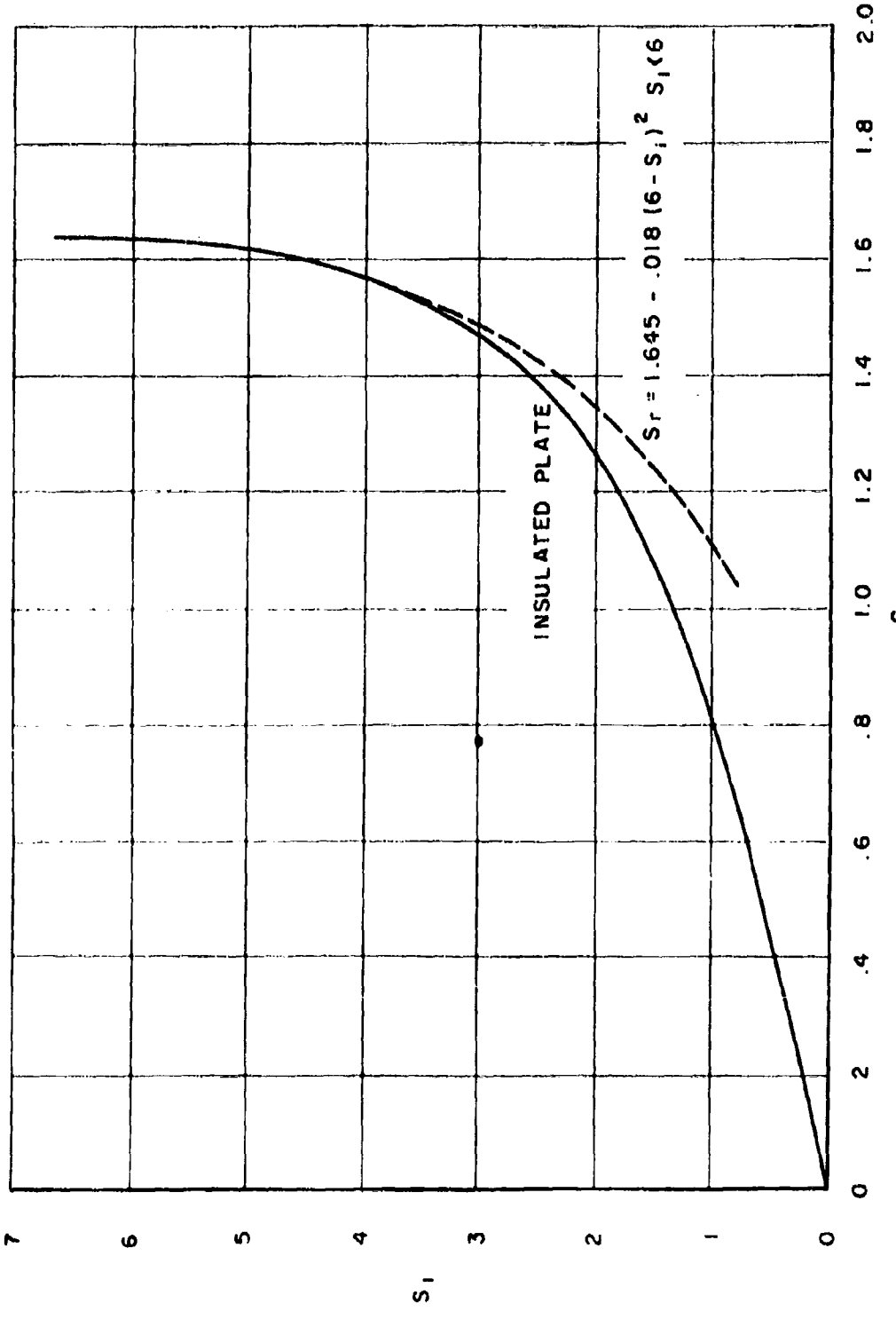

Figure 5. Relation of re-emission speed ratio to incident speed ratio on an insulated cylinder

than two, some type of transition flow such as slip flow occurs until continuous flow is reached at Knudsen numbers of about $K_n = 0.02$ for orbital vehicles. This transition region will most likely begin as the satellite is still orbiting. As an example, the transition point ($K_n = 2.0$) for the Discoverer satellites is at about 130 km. Below 130 km drag coefficients based on experiment or one of the theories such as those which include one collision between air molecules would be used. In any case, the general trend is to decrease the drag coefficient from the free molecular condition. As will be mentioned later, at an altitude of 130 km, the satellite is about to begin its terminal phase. Numerical calculation using free molecular flow drag coefficients indicates the satellite traverses 3/4 or less of an orbit in descending from 130 to 90 km (see Figure 24). The error involved in using free molecular drag coefficients in place of the more realistic slip or continuum flow could not cause an error greater than two revolutions. This is usually negligible for lifetime predictions. On the other hand, if an impact point is desired, the more exact drag coefficients will have to be used.

The basic assumption of free molecular flow is that the air molecules have a Maxwellian velocity distribution superimposed upon the uniform mass velocity. Then, by neglecting collisions between molecules, the flux incidence upon a given area is computed. A drag force also occurs in the reflection of molecules at the surface. It is necessary, however, to make an estimate of the surface conditions in order to predict the mode of reflection. Usually a combination of specular and diffuse reflection occurs. The drag coefficients for four commonly encountered shapes are described below.

i. Sphere

With specular reflection from the surface, the free molecular drag coefficient for a sphere based upon the frontal area is

$$C_{D_s} = \frac{2S^2 + 1}{\sqrt{\pi}\, S^3} \exp(-S^2) + \frac{(4S^4 + 4S^2 - 1)}{2S^4} \operatorname{erf}(S) \qquad (2.12)$$

For a diffuse reflecting sphere

$$C_{D_d} = \frac{(2S^2 + 1)}{\sqrt{\pi}\, S^3} \exp(-S^2) + \frac{(4S^4 + 4S^2 - 1)}{2S^4} \operatorname{erf}(S) + \frac{2\sqrt{\pi}}{3S_r} \tag{2.13}$$

where S_r is the re-emitted speed ratio.

The combined drag coefficient is

$$C_D = C_{D_s} + R\,\frac{2}{3}\,\frac{\sqrt{\pi}}{S_r} \tag{2.14}$$

where R is the proportionality constant between diffuse and specular reflections. In general, this coefficient is assumed to have a value between 0.8 and 1.0.

ii. Flat plate

Though no satellites presently in orbit are approximated as flat plates, nevertheless certain portions of the satellites are flat. As an example, the tumbling cylinder will at frequent intervals project a flat end to the airstream.

The drag coefficients for a flat plate at an angle of attack, α, with the wind velocity vector is

$$C_{D_s} = \sin A \left[\frac{4}{\sqrt{\pi}\, S} \sin A \exp(-S^2 \sin^2 A) + 4\left(\sin^2 A + \frac{1}{2S^2}\right) \operatorname{erf}(S \sin A) \right] \tag{2.15}$$

and

$$C_{D_d} = \frac{2}{\sqrt{\pi}\, S} \exp(-S^2 \sin A) + 2\sin A\left(1 + \frac{1}{2S^2}\right) \operatorname{erf}(S \sin A) + \frac{\sqrt{\pi}}{S_r} \sin^2 A \tag{2.16}$$

The total drag coefficient is

$$C_D = R\,C_{D_d} + (R-1)C_{D_s} \tag{2.17}$$

iii. Cylinder transverse to the flow

The most important basic shape which closely resembles many presently orbiting satellites is the cylinder.

The drag coefficient resulting from flow transverse to the cylinder based on the frontal area is described below.

$$C_{D_d} = \frac{\sqrt{\pi}}{S}\exp\left(-\frac{S^2}{2}\right)\left\{I_0\left(\frac{S^2}{2}\right) + \frac{(1+2S^2)}{2}\left[I_0\left(\frac{S^2}{2}\right) + I_1\left(\frac{S^2}{2}\right)\right]\right\} + \frac{\pi^{3/2}}{4S_r} \tag{2.18}$$

$$C_{D_s} = \frac{2\sqrt{\pi}}{3S}\exp\left(-\frac{S^2}{2}\right)\left[(3+2S^2)I_0\left(\frac{S}{2}\right)^2 + (1+2S^2)I_1\left(\frac{S^2}{2}\right)\right] \tag{2.19}$$

As in all cases, the total drag is

$$C_D = R\,C_{D_d} + (R-1)C_{D_s} \tag{2.20}$$

iv. Prolate ellipsoid

This shape resembles some of the re-entry cones and may be useful at times. The surface area of a prolate ellipsoid is expressed as

$$A = \int C^2\left[(\zeta^2-\eta^2)(\zeta^2-1)\right]^{1/2}\,d\eta\,d\phi \tag{2.21}$$

$$C_{D_{specular}} = \frac{16}{\sqrt{2\pi\gamma}} \frac{c}{b} \frac{1}{S^2} \left\{ \int_0^{\pi/2} \left(\frac{a^2}{c^2} - \cos^2\theta \right)^{1/2} \sin\theta \cos\theta \left[\sqrt{\frac{2}{\gamma}} (1 + \right.\right.$$

$$\left.\left. + \gamma S^2 \cos^2\theta) \operatorname{erf} \left(\sqrt{\frac{\gamma}{2}} S \cos\theta \right) \right] + S \cos\theta \exp\left(\frac{\gamma}{2S^2} \cos^2\theta \right) d\theta \right\}$$

$$C_{D_{diffuse}} = \frac{8}{\sqrt{2\pi\gamma}} \frac{1}{S_1^2} \frac{c}{b} \left\{ \int_0^{\pi/2} \left(\frac{a^2}{c^2} - \cos^2\theta \right)^{1/2} \sin\theta \left[\cos\theta \left(1 + \right.\right.\right. \tag{2.22}$$

$$\left.\left.\left. + \gamma S^2 \sqrt{\frac{2}{\gamma}} \operatorname{erf} \right) \left(\sqrt{\frac{\gamma}{2}} M \cos\theta \right) + S_r \exp\left(-\frac{\gamma}{2} M_r^2 \cos^2\theta \right) \right] d\theta \right.$$

$$\left. + \sqrt{\frac{\gamma\pi}{8}} \frac{c}{b} \frac{1}{M_r} \left[\frac{a^2}{8c^2} \left(\frac{b}{c} + \frac{a^2}{c^2} \sin^{-1} \frac{c^2}{a^2} \right) - \frac{1}{4} \frac{b^3}{c^3} \right] \right\}$$

The drag coefficients for the four basic shapes have been presented in terms of the molecular speed ratio and the satellites projected area. What is generally done is to linearize the functional representations by assuming $S >> 1$. This corresponds to hypersonic flow and approaches the Newtonian theory. This assumption is only valid if the accuracy desired is to the order of the orbital eccentricity. For higher order accuracy, such as that of e^2 or higher, it is essential that more exact representations of the free molecular drag coefficients be employed.

The form of the drag coefficient is only a part of the difficulty encountered in analyzing the satellite drag. The orientation of the satellite itself is also important. However, when the hypersonic flow assumption is made, the drag coefficient per unit frontal area is identical for the sphere, cone, and cylinder. Thus, when the analysis is only to order of the eccentricity, the satellite orientation is not important. In the attempt at refining the satellite decay predictions, higher order terms are included in the orbit equations and in keeping with this increased precision, the satellite orientation as well as the complete expression for the drag coefficient must

be indicated. In the following paragraphs attention will be given to evaluating the drag coefficient on an actual satellite.

The most evident way to begin is to analyze the space and earth stabilized satellites. At one time it was thought that a satellite could be stabilized in space in much the same manner as a gyroscope. This assumption was not upheld, as was proved by the observation of the rapid motion of the spin axis of Explorer IV about the celestial sphere. This posed a dilemma for photographing the earth from Tiros I. It has been substantially demonstrated (Ref. 3) that effects of differential gravity forces cannot be neglected and are the cause for the secular motion of the spin axis. The spin axis in Explorer IV was observed to move as much as three degrees per day and to have reached a maximum deviation from the initial orientation of 15 degrees on the celestial sphere. In addition to the gravity torque there can also be a magnetic torque acting on the satellite's span axis. It is safe to say, serious secular movements of the spin axis of a stabilized satellite do occur which will influence the drag and consequently the decay of the satellite.

As an instructive example nevertheless, consider a space stabilized satellite. The importance of the satellite orientation will then be demonstrated. Consider a satellite such as 1958 Zeta which is an Atlas missile. Assume this satellite to be spin-stabilized with the spin vector aligned with the flight path at the initial perigee point. Approximately one week later, the perigee will have regressed some 58 degrees. Referring to Sketch 1 below, it can be seen that the drag coefficient will have a value somewhere between the two extremes. A way of representing the actual drag would be to assume that the drag coefficient depends upon the argument of the perigee.

$$C_D = C_{D_{min}} + \left(C_{D_{max}} - C_{D_{min}} \right) \left| \cos (\omega_0 - \omega) \right| \qquad (2.23)$$

For this particular example

$$C_D = 1.70 + 0.65 \left| \cos(\omega_0 - \omega) \right| \qquad (2.24)$$

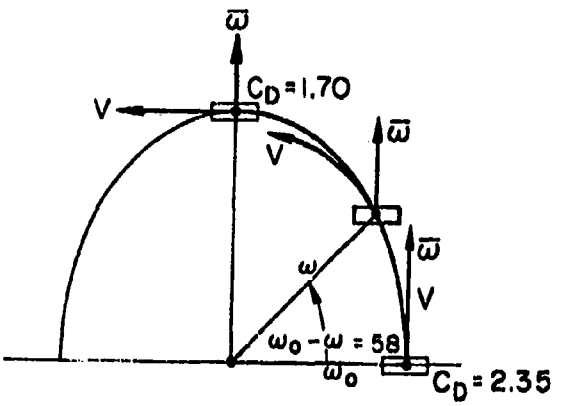

Sketch 1

The motion of the argument of the perigee obviously can attribute a maximum error of 19 per cent on the 150th revolution when $\omega_0 - \omega = 90$ degrees. This should show that the drag coefficient is dependent upon the orbital elements and should not be included as a constant.

To a much lesser degree, the same can be said for an earth-stabilized satellite. In this case however, the body axis will move with respect to the velocity vector only a few degrees during the portion of high drag encounter. This example closely approximates the concept of a constant area and drag coefficient.

(c) Estimation of lift coefficient

In addition to the drag, lift in many instances will also be present. Depending upon the vehicle orientation relative to the wind velocity, the lift will act to either increase or decrease the centripetal force. Generally, it will also have a component in the direction of the side and drag forces. The drag due to lift will usually be a small fraction of the total drag. Even though the side force due to lift is also small, it can create serious

perturbation in the orbital motion. This section will deal with the magnitude of the lift coefficient and determine the effect it has on the side and drag forces.

The first consideration is of a stabilized satellite. The orientation of the vehicle in this instance will be fixed in space. Consider the axis system of Sketch 2:

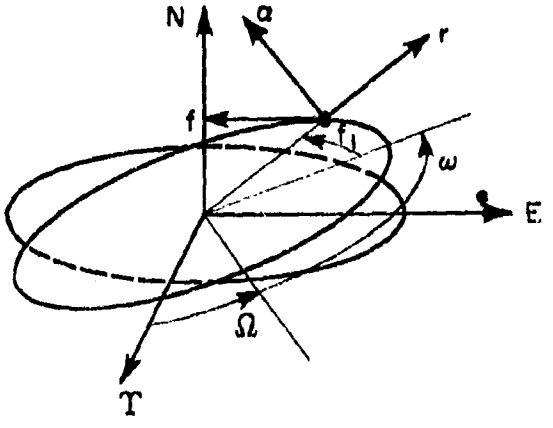

Sketch 2

The satellite orientation is in reference to the r, f, α coordinates. For a spin-stabilized satellite, the angular momentum vector,

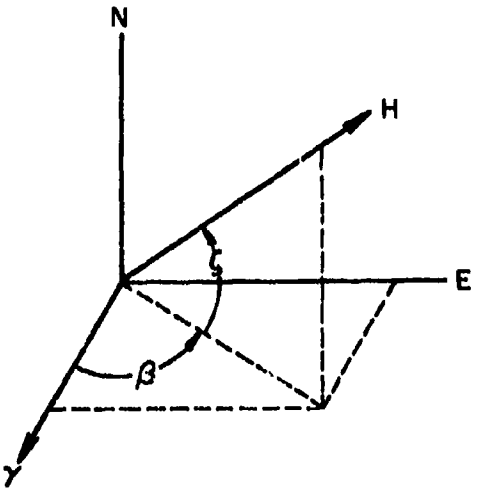

If, is fixed in space.

The momentum vector is located with respect to the N-E-γ inertial axis. Using Euler axis transformation, the momentum vector can be specified in terms of the α-ω-Ω axis. The transformation is as follows on the next page.

$$\begin{pmatrix} H_{\gamma_1} \\ H_{E_1} \\ H_{N_1} \end{pmatrix} = \begin{pmatrix} \cos\Omega & \sin\Omega & 0 \\ -\sin\Omega & \cos\Omega & 0 \\ 0 & 0 & 1 \end{pmatrix} \begin{pmatrix} H_{\gamma} \\ H_{E} \\ H_{N} \end{pmatrix}$$

$$\begin{pmatrix} H_{\gamma_2} \\ H_{E_2} \\ H_{N_2} \end{pmatrix} = \begin{pmatrix} \cos\omega & 0 & -\sin\omega \\ 0 & 1 & 0 \\ \sin\omega & 0 & \cos\omega \end{pmatrix} \begin{pmatrix} H_{\gamma_1} \\ H_{E_1} \\ H_{N_1} \end{pmatrix}$$

$$\begin{pmatrix} H_{\Omega} \\ H_{\omega} \\ H_{\alpha} \end{pmatrix} = \begin{pmatrix} 1 & 0 & 0 \\ 0 & \cos\alpha & \sin\alpha \\ 0 & -\sin\alpha & \cos\alpha \end{pmatrix} \begin{pmatrix} H_{\gamma_2} \\ H_{E_2} \\ H_{N_2} \end{pmatrix}$$

The momentum vector has now been located with respect to the orbit perigee. Further transformations are required to locate it in terms of the actual satellite position. The satellite is located in the orbital plane by the angular measure from the perigee. In this regard

$$\begin{aligned} H_r &= \cos f \; H_{\omega} + \sin f \; H_{\Omega} \\ H_f &= \cos f \; H_{\omega_o \Omega_o} - \sin f \; H_{\omega} \end{aligned} \qquad (2.25)$$

The angular momentum vector has now been located with respect to the satellite position. The velocity vector is also located with respect to the instantaneous satellite position as

$$\begin{aligned} V_r &= \dot{r} \\ V_f &= V_{\phi} - r\,\Omega_{\oplus}\, e \cos\alpha \\ V_{\alpha} &= r\,\Omega_{\oplus}\, e \sin\alpha \cos\phi \end{aligned} \qquad (2.26)$$

The angle of attack, yaw, and roll can now be determined as the angle between momentum and velocity vectors. The angle of attack is

$$A = \frac{\vec{V}_f \cdot \vec{H}_f}{|V_f| \cdot |H_f|} \tag{2.27a}$$

Similarly, the angles of roll and yaw are

$$\text{yaw} \equiv B = \frac{\vec{V}_r \cdot \vec{H}_r}{|V_r| \cdot |H_r|} \tag{2.27b}$$

$$\text{roll} \equiv C = \frac{\vec{V}_\alpha \cdot \vec{H}_\alpha}{|V_\alpha| \cdot |H_\alpha|} \tag{2.27c}$$

Lift forces can be created on unsymmetric shapes. One usually thinks of the flat plate or cone at an angle of attack. Following the same presentation as for drag, the lift coefficient for diffuse reflection from a flat plate is

$$C_{L_d} = \frac{\cos A}{S^2} \operatorname{erf}(S \sin A) + \frac{\sqrt{\pi} \sin A \cos A}{S_r} \tag{2.28}$$

The lift coefficient for the case of specular reflection is

$$C_{L_s} = \cos A \left[\frac{4}{\sqrt{\pi}\, S} \sin A \exp(-S^2 \sin^2 A) + 4\left(\sin^2 A + \frac{1}{2S^2}\right) \operatorname{erf}(S \sin A) \right] \tag{2.29}$$

The actual lift coefficient lies between these two, i.e.,

$$C_L = K' C_{L_d} + (K' - 1) C_{L_s} \tag{2.30}$$

The lifting force is always smaller than the drag force

at moderate molecular speed ratios. As an example, for $S \geq 6$, the $L/D \leqq 0.20$. Though the lift force is small relative to the drag, its effect in the radial direction may be important during the final stages of decay.

2. Perturbing functions

The preceding sections have served to formulate the basic quantities needed to state the force equations. It is the purpose of this section to combine the various factors of gravity, drag and, where applicable, lift into a form amenable for later use in determining the motion of a near-earth satellite. The equations will be written without proof in the orbital plane coordinate system.

$$\frac{F_r}{m} = -\frac{KM}{r^2}\left[1 + J\left(\frac{R_\oplus}{r}\right)^2 (1 - 3\sin^2\phi \sin^2\alpha) - \right.$$

$$\left. - \frac{D}{7}\left(\frac{R_\oplus}{r}\right)^4 (35 \sin^4\phi \sin^4\alpha - 30 \sin^2\phi \sin^2\alpha + 3)\right]$$

$$- \frac{1}{2}\rho V_R\left(\frac{C_D A}{m}\right) \dot{r} + \frac{1}{2}\rho V_r\left(\frac{C_L A}{m}\right)(V_\phi - r\,\Omega_\oplus \cos\alpha)$$

(2.31)

$$\frac{F_\phi}{m} = -\frac{2JKMR_\oplus^2}{r^4} \sin\phi \cos\phi \sin^2\alpha - \frac{D}{7}\frac{R_\oplus^4}{r^6} KM\left[28 \sin^4\alpha \sin^3\phi \cos\phi - \right.$$

$$\left. - 12 \sin^2\alpha \sin\phi \cos\phi\right] - \frac{1}{2}\rho V_{R_\oplus}\left(\frac{C_D A}{m}\right)(V_\phi - r\,\Omega_e \cos\alpha) +$$

$$+ \frac{1}{2}\rho V_{R_\oplus}\left(\frac{C_L A}{m}\right) \dot{r}$$

$$\frac{F_\alpha}{m} = -\frac{2JR_\oplus^2}{r^4} KM \sin\phi \cos\alpha \sin\alpha - \frac{D}{7}\frac{R_\oplus^4}{r^6} KM [28 \sin^3\phi \sin^3\alpha \cos\alpha -$$

$$- 12\sin\phi \sin\alpha \cos\alpha] - \frac{1}{2}\rho V_R(r\Omega_\oplus \sin\alpha \cos\phi)\left(\frac{C_D A}{m}\right)\left(1 - \frac{C_L}{C_D}\right)$$

III. EQUATIONS OF MOTION FOR A NEAR-EARTH SATELLITE

The force terms and the perturbing functions have been developed in the preceding section and are now to be equated to the rate of change of momentum. In general, the equations of motion in spherical coordinates are given as

$$\begin{aligned} \ddot{r} - \frac{V_\phi^2}{r} &= \frac{F_r}{m} \\ \left(\dot{V}_\phi + \dot{r}\frac{V_\phi}{m}\right) &= \frac{F_\phi}{m} \\ V_\phi \Omega r &= \frac{F_\alpha}{m} \end{aligned} \tag{3.1}$$

where

$$\frac{V_\phi}{r} = \dot{\phi} + \dot{\theta}\cos\alpha \tag{3.2}$$

$$\Omega_r = \frac{\dot{\theta}\sin\alpha}{\sin\phi} \tag{3.3}$$

These equations are non-linear second order differential equations and conceivably could be integrated numerically as they stand. This, however, would be in complete disregard of the brillant work of the classical astronomers. The classical astronomers developed several perturbation techniques which when applied to the equations of motion offer many particular advantages. The prominent special perturbation techniques which are applicable to the motion of a near-earth satellite are Cowell's, Encke's, and variation-of-parameter methods(Cowell's method is not a

perturbation technique but is grouped as such when comparing the relative merits of these three prominent methods).

The choice between the three methods depends upon the particular trajectory to be encountered. Cowell's method, which is a direct integration of the accelerations, is suited for large perturbative forces. For such forces such as rocket thrust, Cowell's method will afford the least number of computations per step but will require many steps (Ref. 11). It has the disadvantage of requiring a large number of significant figures. Encke's method is best suited for moderate perturbations acting only during a segment of the trajectory such as thrust forces applied intermittently while in orbit to provide stabilization or in orbit transfer and turning. Encke's method is a true perturbation technique wherein only the acceleration difference between the actual and reference orbit is integrated. This integration of only the departure from a reference orbit permits using fewer significant figures and larger integration steps. The natural improvement to Encke's method was the use of a continuously changing reference orbit. This is known as the variation-of-parameter method and is suited for small perturbation forces acting throughout the orbit. This method permits large integration steps but the computations are extensive in each step. As this study is concerned with the satellite's motion near and at its demise, the variation-of-parameter method affords the minimum of computational time and has flexibility and control of the associated computational errors.

The variation-of-parameter method is the computation technique used in this study. The reference motion of the satellite is represented by a set of orbit parameters which, in the absence of the drag forces, would be constant from revolution to revolution. The drag forces, however, cause these parameters to vary, and the differential equations of motion are derived from these parameters. These differential equations are then integrated to describe the satellite motion. The description of the reference orbit is provided in the following paragraphs.

The reference orbit, sometimes referred to as an oscillating or instantaneous ellipse, is specified by three parameters. In place of the usual eccentricity and semi-major axis, the dimensionless parameters

p and q are used. The parameter p is the semi-latus rectum of the oscillating ellipse and also represents the product of velocity and radius.

$$P = \frac{L_0}{a(1 - e^2)} \tag{3.4}$$

where

$$L_0 = \frac{(r_0 V_\phi)^2}{KM} \tag{3.5}$$

Also,

$$P = \left(\frac{r_0 V_{\phi_0}}{r V_\phi} \right)^2 \tag{3.6}$$

The second parameter, q, is a product of the eccentricity and semi-latus rectum.

$$q = P e \tag{3.7}$$

One other parameter is required to completely specify the reference ellipse. This is the angle ω which locates the argument of the perigee with respect to some reference direction. The relation of ω to the polar angle and argument of the perigee is indicated below and in Figure 6.

$$\omega = \phi - f \tag{3.8}$$

where f is the true anomaly, the angular displacement in the orbit plane measured from the perigee.

The orientation of the reference orbit in space remains to be specified. This is conventionally done by specifying the angle of inclination α, the line of ascending node Ω, and the epoch time. These six orbital elements completely specify the dynamical state of the satellite and inherently require the momentum and the energy associated in the reference ellipse to be identical with those of the actual trajectory.

The second order differential equations of motion (3.1) have an equivalent form as six first order differential equations in the oscillating elements. In terms of these elements, the equations of motion in the oscillating elements are given (Ref. 13) as

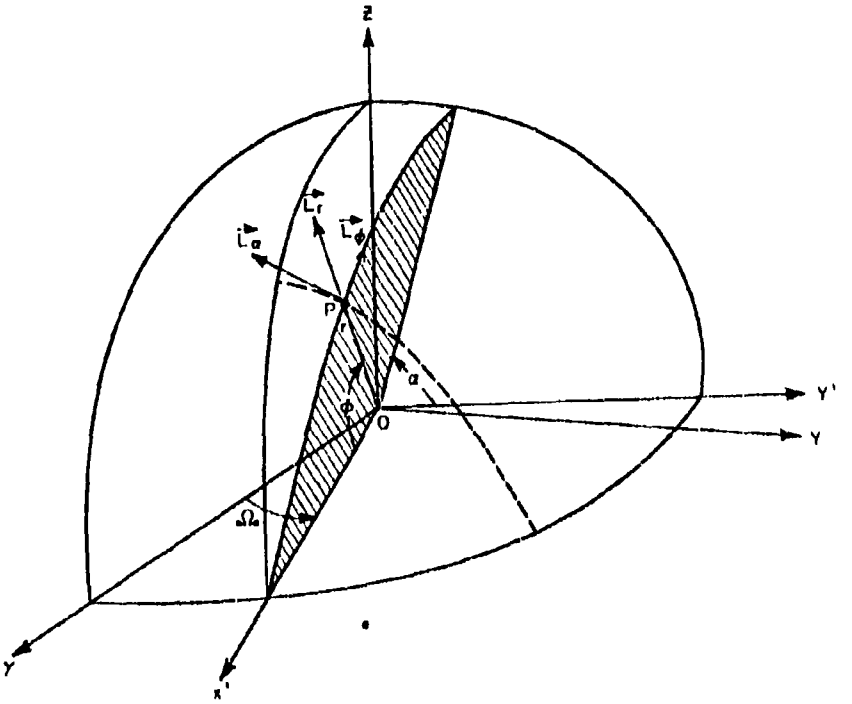

Figure 6a. Trajectory coordinates

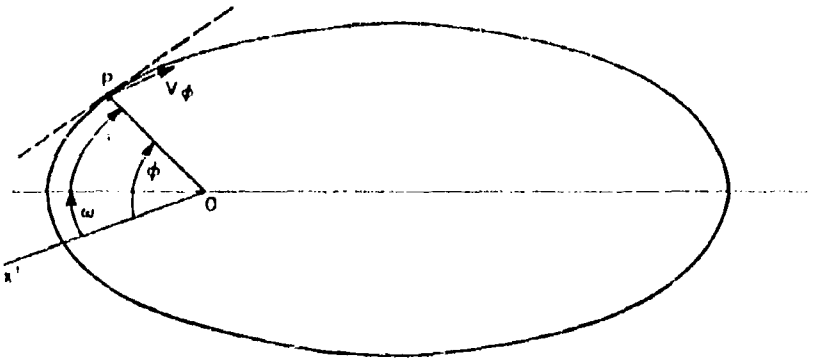

Figure 6b. Instantaneous ellipse coordinates

$$
\left.
\begin{aligned}
&\text{(a)} \quad \frac{dt}{d\phi} = \frac{1}{\dot{\phi}} = \frac{1}{\frac{V_\phi}{r} - \left(\frac{F'_\alpha}{m}\right)\frac{\sin\phi\cos\alpha}{V_\phi}} \\
&\text{(b)} \quad \frac{dP}{d\phi} = -\frac{2P}{\dot{\phi}V_\phi}\left(\frac{F_\phi}{m}\right) \\
&\text{(c)} \quad \frac{d\Omega}{d\phi} = \frac{\sin\phi}{\dot{\phi}V_\phi}\left(\frac{F'_\alpha}{m}\right) \\
&\text{(d)} \quad \frac{d\alpha}{d\phi} = \frac{\cos\phi}{\dot{\phi}V_\phi}\left(\frac{F_\alpha}{m}\right) \\
&\text{(e)} \quad \frac{dq}{d\phi} = -\frac{dP}{d\phi}\cos f + S_1 \sin f \\
&\text{(f)} \quad \frac{d\omega}{d\phi} = -\frac{d\Omega}{d\phi}\cos\alpha - \frac{1}{q}\frac{dP}{d\phi}\sin f - \frac{S_1}{q}\cos f
\end{aligned}
\right\} \qquad (3.9)
$$

where the quantity S_1 is defined as

$$
S_1 = \frac{1}{2P}\frac{dP}{d\phi}\, q \sin f + P\left[\frac{r^2}{KM}\left(\frac{F_r}{m}\right) + 1\right]\left(1 + \frac{d\Omega}{d\phi}\cos\alpha\right)
$$

These six differential equations have been programmed for an IBM 704 with the following auxiliary equations.

$$
V_\phi^2 = \frac{KM}{r}\left[1 + J\frac{R^2}{r^2}\left(1 - 3\sin^2\phi\sin^2\alpha\right)\right]\left[\frac{1 + 2e\cos f + e^2}{1 + e\cos f}\right]
$$

$$
\dot{r} = \frac{rV_\phi q}{L_0}\sin f
$$

$$
V_R^2 = \dot{r}^2 + (V_\phi - r\Omega e\cos\alpha)^2 + (r\Omega e\sin\alpha\cos\phi)^2
$$

$$
\frac{F'\alpha}{m} = \frac{F\alpha}{m}\,\frac{1}{\sin\alpha}
$$

These equations when programmed along with the various subroutines for evaluating the drag coefficient and density provide the numerical solution to the equations of motion. The variation-of-parameter method employed does have the disadvantage of singularities for the case of circular orbits (e = 0). The equations so chosen have as the independent variable the polar angle ϕ which is in effect the true anomaly. At the terminal phase of the satellite trajectory where the motion is nearly vertical, this independent variable is a poor choice since small changes in it are accompanied by large changes in the dependent variable. This however will occur below 100 km and for all purposes the satellite has ceased orbiting. In view of this, the equations are not altered.

IV. NUMERICAL SOLUTION

The equations of motion (3.9) and the various auxiliary equations have been programmed for an IBM 709 using Fortran language. The differential equations are integrated using the Adams-Moulton, Runge-Kutta technique (Ref. 12). This subroutine integrates a set of N simultaneous, first order differential equations. The choice of this subroutine lies in the available option of integration step-size. The Adams-Moulton error-control permits adopting a variable step-size, mode 0, or, a fixed step size, mode 1, both with the fourth order Runge-Kutta integration method. Through the use of a variable step-size, self-determined by the magnitude of round-off error and truncation error permitted, machine time can be saved at no loss of desired accuracy. The user is free to specify the truncation error which is equivalent to specifying the number of significant figures. The round-off error control is achieved with the use of double precision internally. The derivative calculations are performed in single precision.

The variable step-size is limited in range between a lower and upper bound. The lower bound is chosen as a compromise between the desired accuracy and machine time. Usually, the lower bound is chosen 100 times the upper bound. After considerable experience is obtained with the program, the fixed step-size mode 1 can be used which is five

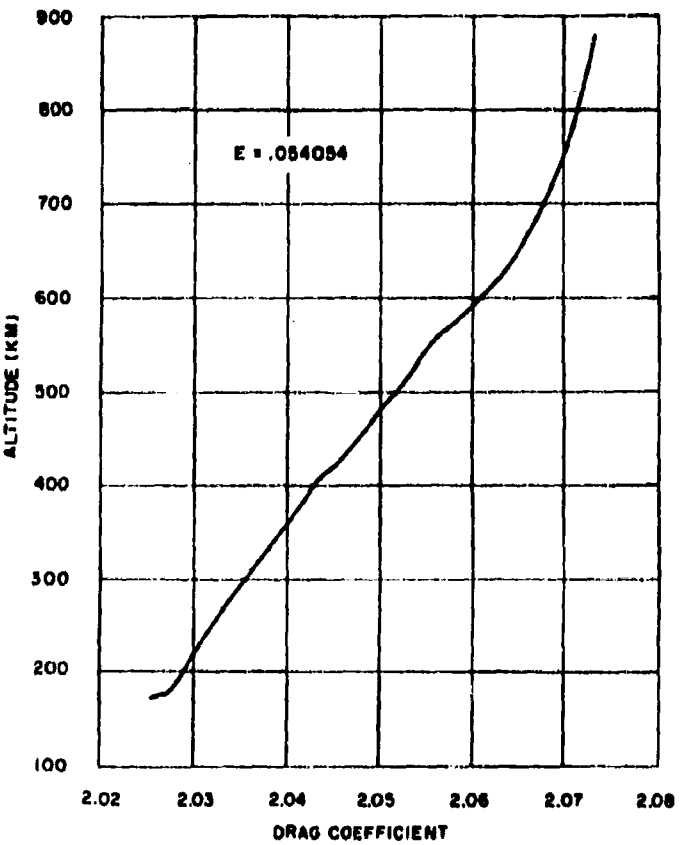

Figure 7. Specular drag coefficient for a sphere as a function of altitude

times faster than the variable mode. Increments as large as 30 degrees have been used with small loss of accuracy, as indicated in the comparison below (Case 1).

	$\Delta\phi = 1°$	$\Delta\phi = 30°$
PHI	12.4349 rad	12.4348 rad
r	6793.8676 km	6793.8723 km
e	0.0150522	0.0150522
c	103.825800 km	103.836909 km
R. A.	5.888034 rad	5.888034 rad
f	521.84 deg	521.84
Drag	0.62285×10^{-5} Newtons/Kg	0.62280×10^{-5} Newtons/Kg
h	416.0819 km	416.0874 km

Increments as large as ninety degrees definitely cannot be used.

The accuracy check is made with an inclined orbit with no drag. The machine is required to repeat all pertinent values for twenty revolutions. This was achieved through the sixth decimal place. Similarly, the rate of change of right ascension and argument of perigee for an orbit with no drag were checked with available values determined from series solutions (Ref. 14) and agreed with the desired accuracy for the second order earth potential. Several cases of results are presented below, (Case 2).

EQUATORIAL ORBIT, $\frac{A}{m} = 0$

f	h	e	V_ϕ	ω	α	$\dot{\Omega}_0$
0	221.8550	0.09999999	8.1569862	0	0	0
1800.000	221.8549	0.01000001	8.1569862	0.078604	0	− 0.0392223
7199.999	221.8552	0.09999999	8.1569860	0.3144434	0	− 0.1569149

POLAR ORBIT, $\frac{A}{m} = 0$

1800.000	221.8703	0.09999724	8.1569718	− 0.0197609	1.5707963	− 0.0000000

POLAR ORBIT, $\frac{A}{m} = 7.5 \times 10^{-4}$ km²/Kg

1800.000	221.7993	0.0997155	8.1559711	− 0.0197676	1.570963	− 0.0000000

The program has the following features. The atmospheric density is obtained from a table rather than an exponential equation. By specifying shape, the decay can be computed for either cylindrical or spherical satellites or for the case of constant drag coefficient. For the spherical or cylindrical satellite, the drag coefficient is computed on the basis of the molecular-scale temperature and specified constant accommodation coefficient. The drag coefficient changes only a few per cent with altitude as can be observed in Figure 7. These few per cent, however, can cause an additional height loss of one kilometer for every ten revolutions as shown below for the Case 3 with $A/m = 1 \times 10^{-7}$ km^2/Kg.

	N = 0	N = 10		
		C_D = 1.8	C_D = 2.0	C_D = 2.1
f	0	3602.74	3602.68	3602.63
r (km)	6578.1450	6566.8535	6564.8657	6563.7740
h (km)	200.0000	188.7886	186.7208	185.6292
e	.0200000	0.0140897.	0.0132895	0.0128726
c (km)	134.247854	93.847324	88.41899	85.514985
R.A.	0	- 0.000004	- 0.000004	- 0.000005
Phi (deg)	0	62.8325	62.8325	62.8325

A much larger effect is shown in the linear eccentricity. For diffuse drag coefficient the variation can be greater depending upon the definition of the re-emission speed ratio.

Normally, interest is shown only for the values of the orbital elements at perigee and apogee. However, at low altitudes, the perigee is ill defined and it becomes necessary to define the orbital elementals at every integration. The altitude for the change in information output can be selected but it has been found to occur no higher than 150 km though it may be lower.

V. AN APPROXIMATE METHOD OF SATELLITE DECAY PREDICTIONS

With the aid of the present computer program, revisions have been made in the approximate satellite decay predictions (Ref. 4). This program has been valuable in evaluating certain functions and determining relationships between orbital elements. A brief review will be made of the approximate method, including the aids furnished from the computing program. A test of the approximate method will also be presented on a number of earth satellites. The results are very favorable.

The basis of the approximate method lies in the law of conservation of energy. The drag force is assumed to occur instantaneously during a given revolution. The energy lost due to the drag is then subtracted from the satellite energy, and the orbital element adjusted to compensate for this loss. The loss of energy per revolution can be expressed as

$$\frac{dE_D}{dN} = -\frac{1}{2} C_D A (V_p q)^2 \exp^{-A_1} \int_0^{2\pi} \frac{\exp^{-r/G}}{r} df \qquad (5.1)$$

The approximations made in the equation are within an order of e^2. The equation employs an exponential density variation. The density scale height, G, is computed from the 1959 ARDC Model Atmosphere (Ref.6) and is plotted in Figure 8. The irregularities between 170 km and 280 km are due to the variation in molecular temperature.

Expressing the orbit radius, r, as

$$r = q + c\,(1 - \cos f) + \mathcal{O}(e^2)$$

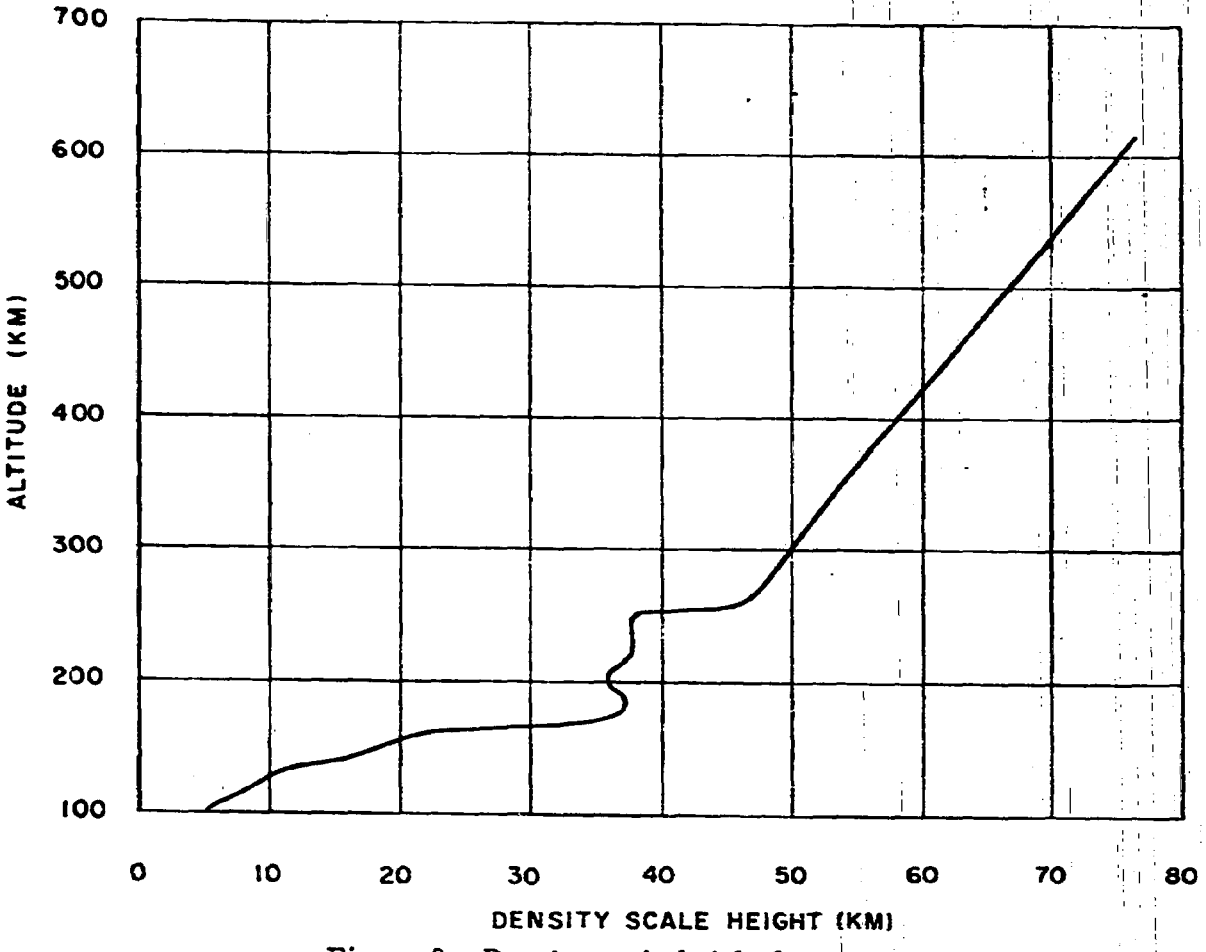

Figure 8. Density scale height for various altitudes

the integral can be evaluated in terms of Bessel's function. The loss of energy per revolution is then shown to be

$$\frac{dE_D}{dN} = \sqrt{\frac{\pi}{2}}\,(C_D A)\,KM\,(1-e)\,\rho\sqrt{\frac{G}{c}}\left\{\frac{\sqrt{2\pi k}\;I_0(k)}{\exp(k)} + \right. \tag{5.2}$$

$$\left. + \frac{\sqrt{2\pi k}\;I_1(k)}{\exp(k)}\left(e + \frac{0.125 - 0.375e}{k}\right) + \cdots\right\}$$

where the argument k represents the product of density scale height, G, and linear eccentricity, c, the terms

$$\frac{\sqrt{2\pi k}\;I_0(k)}{\exp(k)} \text{ and } \frac{\sqrt{2\pi k}\;I_1(k)}{\exp(k)}$$

deviate from unity only as $k \to 0$. For values of $k > 4$, the terms are ≤ 1.01. For $k >> 4$, Equation (5.2) is written as

$$\frac{dE_D}{dN} = \sqrt{\frac{\pi}{2}}\,(C_D A)\,KM(1-e)\,\rho\sqrt{\frac{G}{c}}\left[1 + e + \frac{0.125 - 0.375e}{k}\right] \tag{5.3}$$

To obtain the variation in the orbit due to this energy loss, differentiate the total energy associated with the initial orbit.

$$\frac{dE_0}{dN} = + \frac{K\,Mm}{2(q+c)^2}\left(\frac{dq}{dN} + \frac{dc}{dN}\right) \tag{5.4}$$

Thus a change in orbit energy will affect the perigee height and linear eccentricity. From the two equations, the motion of perigee and linear eccentricity can be evaluated. Frequently, the perigee and linear eccentricity are combined into one parameter, the semi-major axis from which the orbital period is determined.

$$q = a - c \quad , \quad P_f = \frac{2\pi KM}{a^{3/2}} \tag{5.5}$$

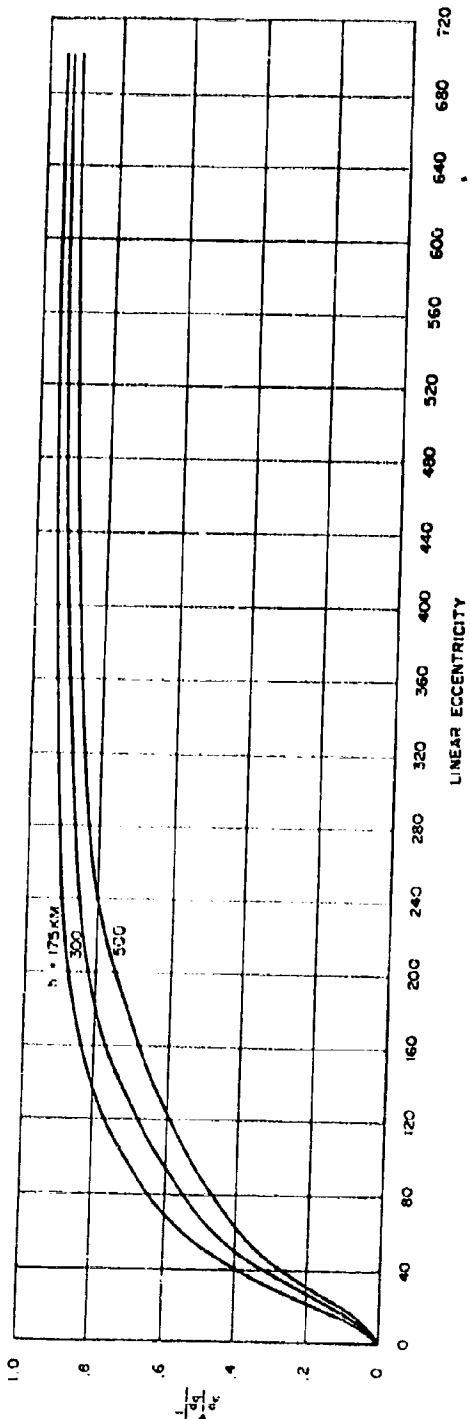

Figure 9. Ratio of change in linear eccentricity to change in perigee as a function of linear eccentricity

$$\frac{dq}{dN} + \frac{dc}{dN} = \frac{da}{dN} = \sqrt{\frac{2\pi G}{c}} \left(\frac{C_D A}{m}\right) pq \left[Q \frac{\sqrt{2\pi k}\, J_0(k)}{\exp(k)} + \frac{\sqrt{2\pi k}}{8Gc} \frac{J_1(k)}{\exp(k)} + \cdots \right] \qquad (5.6)$$

This can be related directly to rate of decrease in orbital period by

$$\frac{dP}{dN} = -\frac{3}{2} \frac{P}{a} \frac{da}{dN} \qquad (5.7)$$

The success of orbit decay predictions based on the rate of decrease in orbital period suggests that the two variables probably are independent for at least large values of linear eccentricity. There is no simple equation which can be used to separate dq/DN and dc/dN. The ratio dq/dc can be approximated with varying orders of accuracy. The important factor about this ratio is its independence from the satellite size and shape, though it does depend upon density. With this in mind the variation of dq/dc with the linear eccentricity was computed numerically using the program outlined previously. The results are plotted in Figure 9 as 1/1 + (dq/dc) which has limits of 0 and 1. This information can be used directly to separate the variables. The next step in forming an approximate equation for predicting decay is integration of Equation (5.6). Integration with limits extending from the initial linear eccentricity to zero or the start of spiral decay, depending upon initial altitude results in Equation (5.8).

$$N_0 - N_s = \sqrt{\frac{1}{2\pi G}} \frac{1}{\rho} \left(\frac{m}{C_D A}\right) \left[1 + e + \frac{0.125 - 0.375e}{Gc} \right] \int_{c_0}^{c_s} \frac{\left(1 + \frac{dq}{dc}\right)\sqrt{c}}{q}\, dc \qquad (5.8)$$

The product $(1 + (dq/dc))\sqrt{c}$ is proportional to $\sqrt{e}$ for all values of $c \geq 150$. So in fact, dq and dc are independent for all values of $c \geq 150$. As will be shown later, values of $c < 150$ are obtained only near the very end of the satellite lifetime.

The orbital lifetime is obtained after further integration and is expressed as

$$N_s - N_0 = \frac{1}{2} \sqrt{\frac{c}{2\pi G}} \left(\frac{m}{C_D A}\right) \frac{e}{pq} \quad , \quad c > 150 \qquad (5.9)$$

The density parameter, $\rho\sqrt{G}$, for various altitudes is presented in Figure 10.

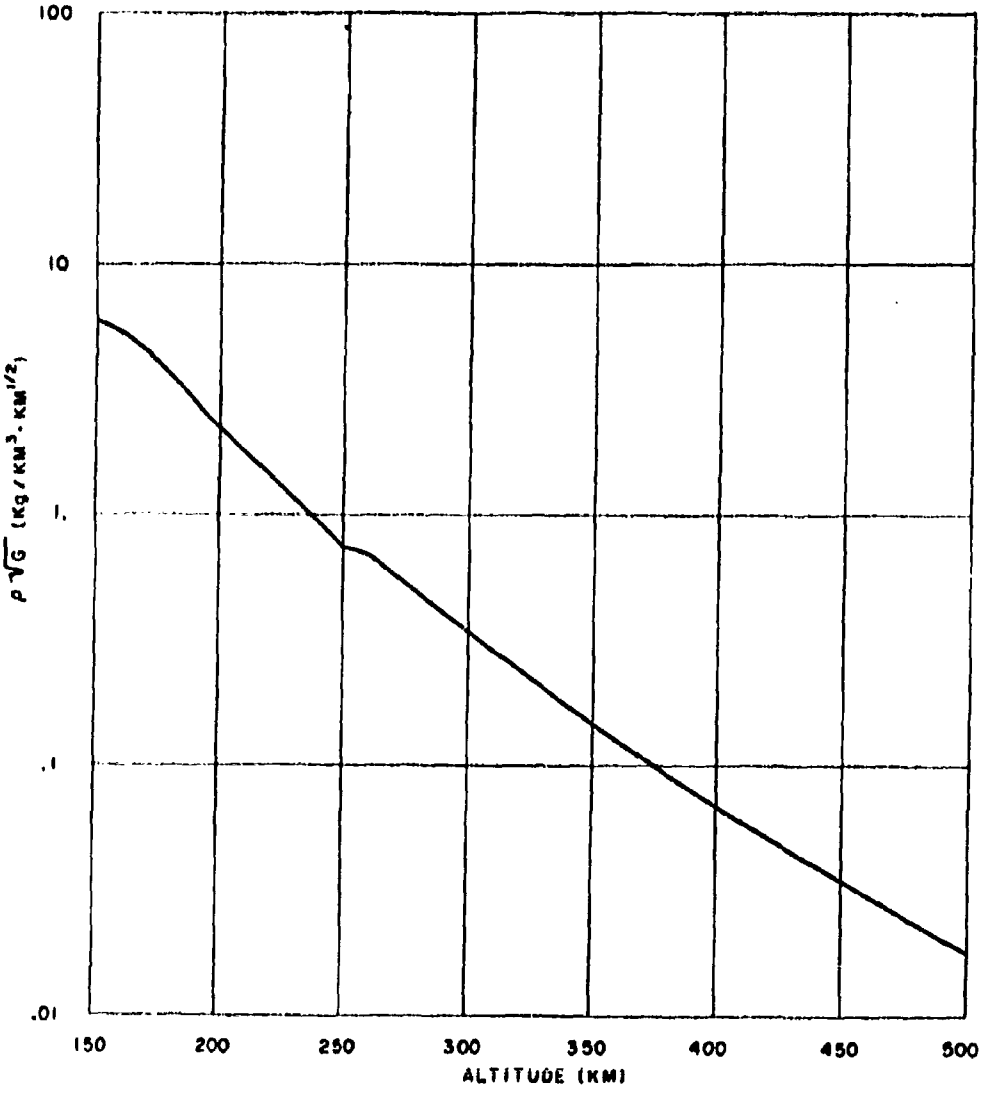

Figure 10. Satellite decay density parameter

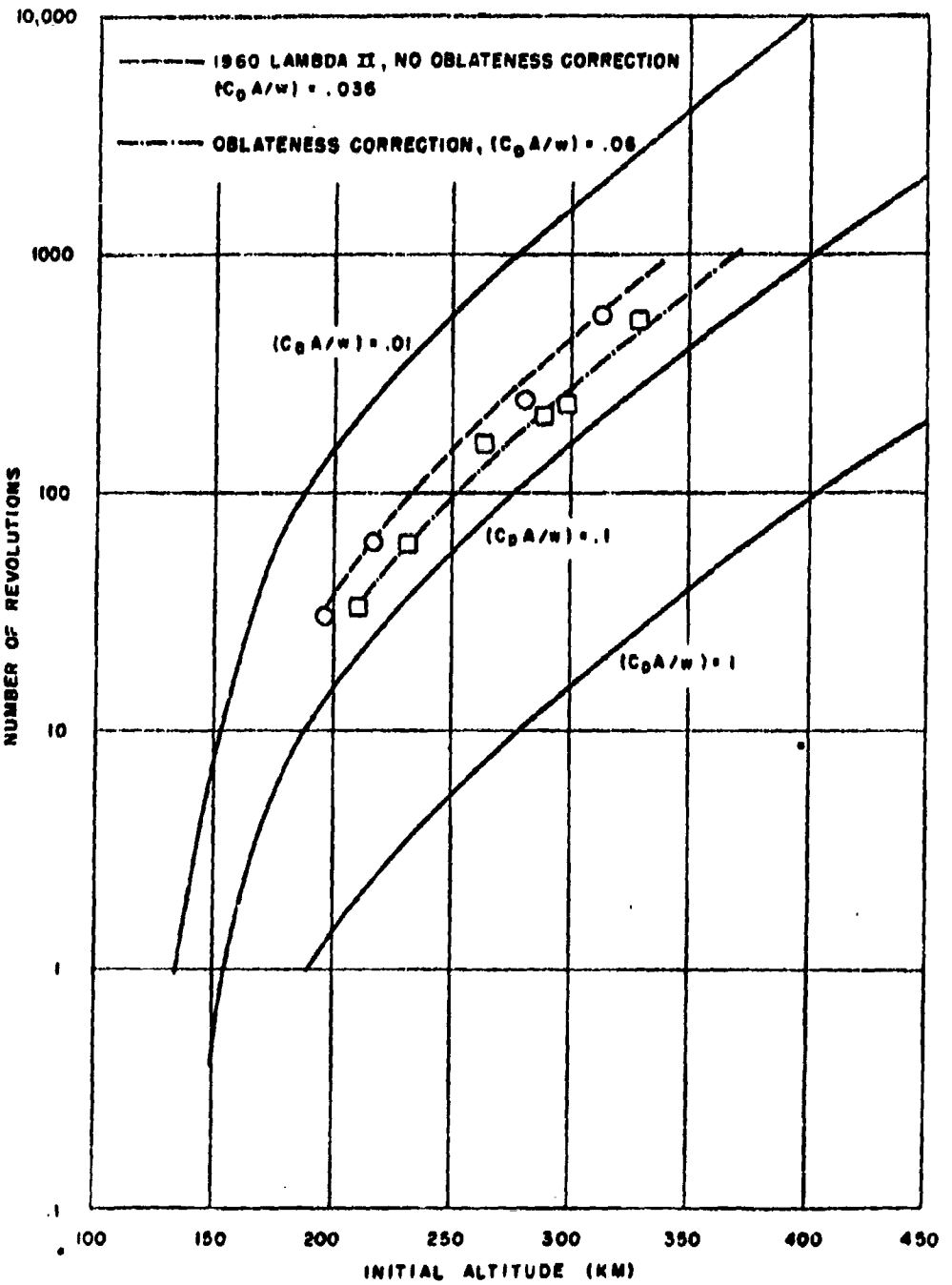

Figure 11. Lifetime of an earth satellite in a circular orbit

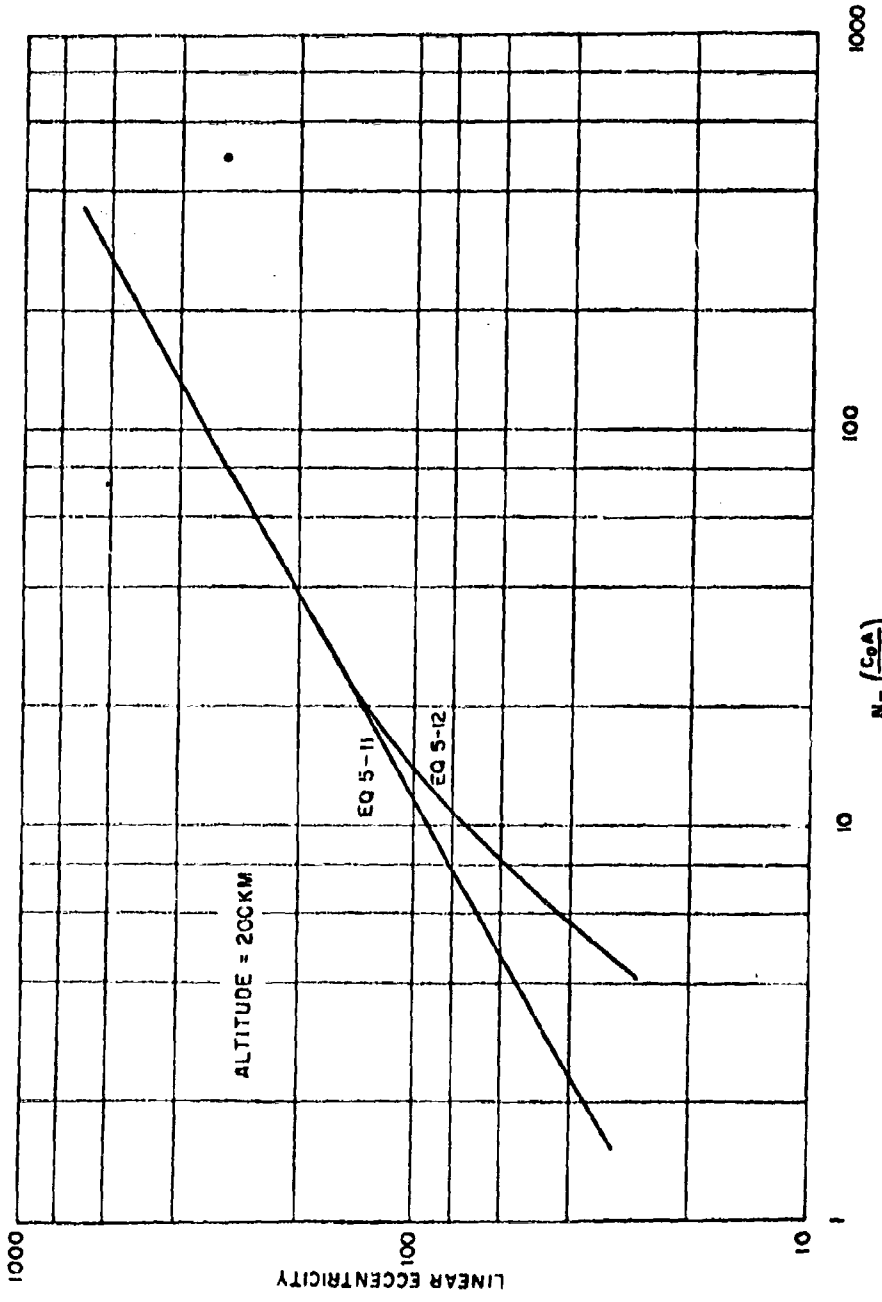

Figure 12. Straight line approximation to linear eccentricity vs $N_s\left(\frac{C_D A}{W}\right)$

An independent exact solution is possible for the asymptotic case of c = 0. For the circular orbit,

$$\frac{C_D A}{m} N_0 = \int_{r_1}^{r_2} \frac{dr}{r^2 \rho} \tag{5.10}$$

The solution is plotted in Figure 11 for a family of load factors. In this figure the load factor of Sputnik V rocket was determined. The effect of the earth's oblateness on the altidude of the satellite has an important effect upon the ballistic coefficient value determined.

A measure of the validity of any assumption is in the result. For the case of Equation (5.8), it was found in comparing the actual satellite's motion and the machine computations, that the prediction became poorer as the linear eccentricity increased. It was first thought that since only terms of order e were used, the equation should not be expected to be useful beyond 600 or 800 revolutions. It was found, however, than an empirical factor of $(c/100)^{0.366}$ could be included in Equation (5.8) which then resulted in good agreement with decayed satellites. The empirically corrected equation is then

$$N_T = \frac{1}{2} \sqrt{\frac{c}{2\pi G}} \left(\frac{m}{C_D A}\right) \frac{e}{\rho q} \left(\frac{c}{100}\right)^{0.366} \qquad c > 150 \tag{5.11}$$

This equation has been plotted in Figure 12. With either Figure 12 or Equation (5.11), the satellite lifetime and load factor can be determined using two values of linear eccentricity separated by a known number of revolutions.

In the absence of reliable satellite data at low eccentricities, machine computations were used to evaluate Equation (5.11). Equation (5.11)was found to predict too few a number of revolutions. This could be corrected by using the (1 + dq/dc) factor which must be corrected to equal zero at c > 200. The final equation is

$$N_T = \frac{1}{2.2} \sqrt{\frac{c}{2\pi G}} \left(\frac{m}{C_D A}\right) \frac{e}{\rho q} \left(\frac{c}{100}\right)^{0.366} \left(1 + \frac{dq}{dc}\right) \tag{5.12}$$

This equation agreed with numerical calculations and satellite data at all values of linear eccentricity. In Figure 12, a comparison is made of Equations (5.11) and (5.12). It is seen they are identical for c > 150 as expected. The nonlinear term in Equation (5.12) is the source of longer lifetime at low eccentricities than predicted by linearized theory.

Equation (5.12) is also plotted in Figure 14 using a larger scale in order to show the motion of 1961 Zeta and 1959 Epsilon II. These two objects were plotted according to their observed altitude and linear eccentricity. In this comparison and others which follow, the source of information is the Space Track Bulletins. It should be recognized that this orbit information is preliminary and in most cases is revised after more observations are received and further analysis made. The revised orbit information, however, usually lags far behind the satellite's lifetime. The working analysis should, therefore, be designed for the preliminary data.

The approximate equation (5.12) as fitted to satellite data is plotted in Figures 13 and 14 as a function of linear eccentricity. The result is a family of curves for each of the various altitudes. There is a slight decrease in slope at low eccentricities with increasing altitudes. The nonlinear term added at low eccentricities is a function of altitude. The family of curves can be reduced to a single curve, excluding the nonlinear term, using the normalizing height factor as plotted in Figure 15. Slight corrections are present for low eccentricities.

Since it has been possible to collapse the family of curves into one curve, the total number of revolutions and ballistic coefficient can be separated. Using curves of total number of revolutions versus linear eccentricity the ballistic coefficient can be determined. This has been done in Figure 16 for a large number of satellites. The ballistic coefficients for each satellite is listed in Table 5-1.

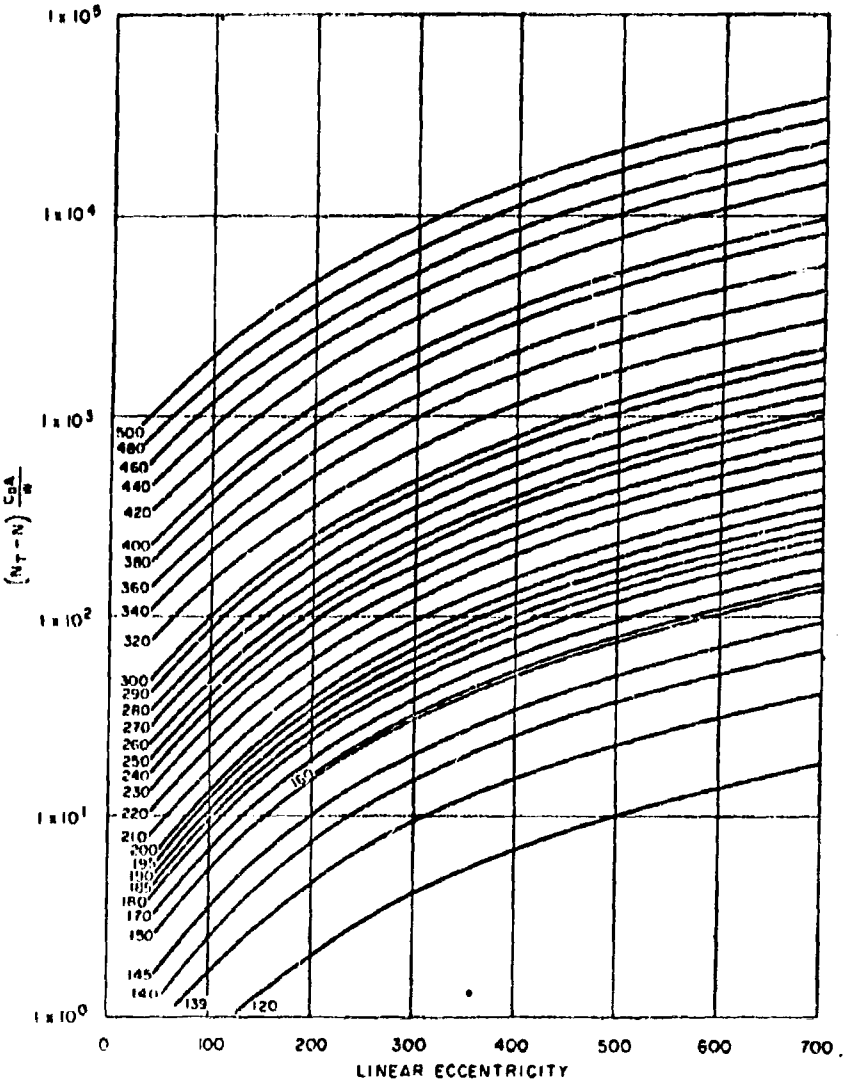

Figure 13. Satellite lifetime prediction as a function of altitude and linear eccentricity

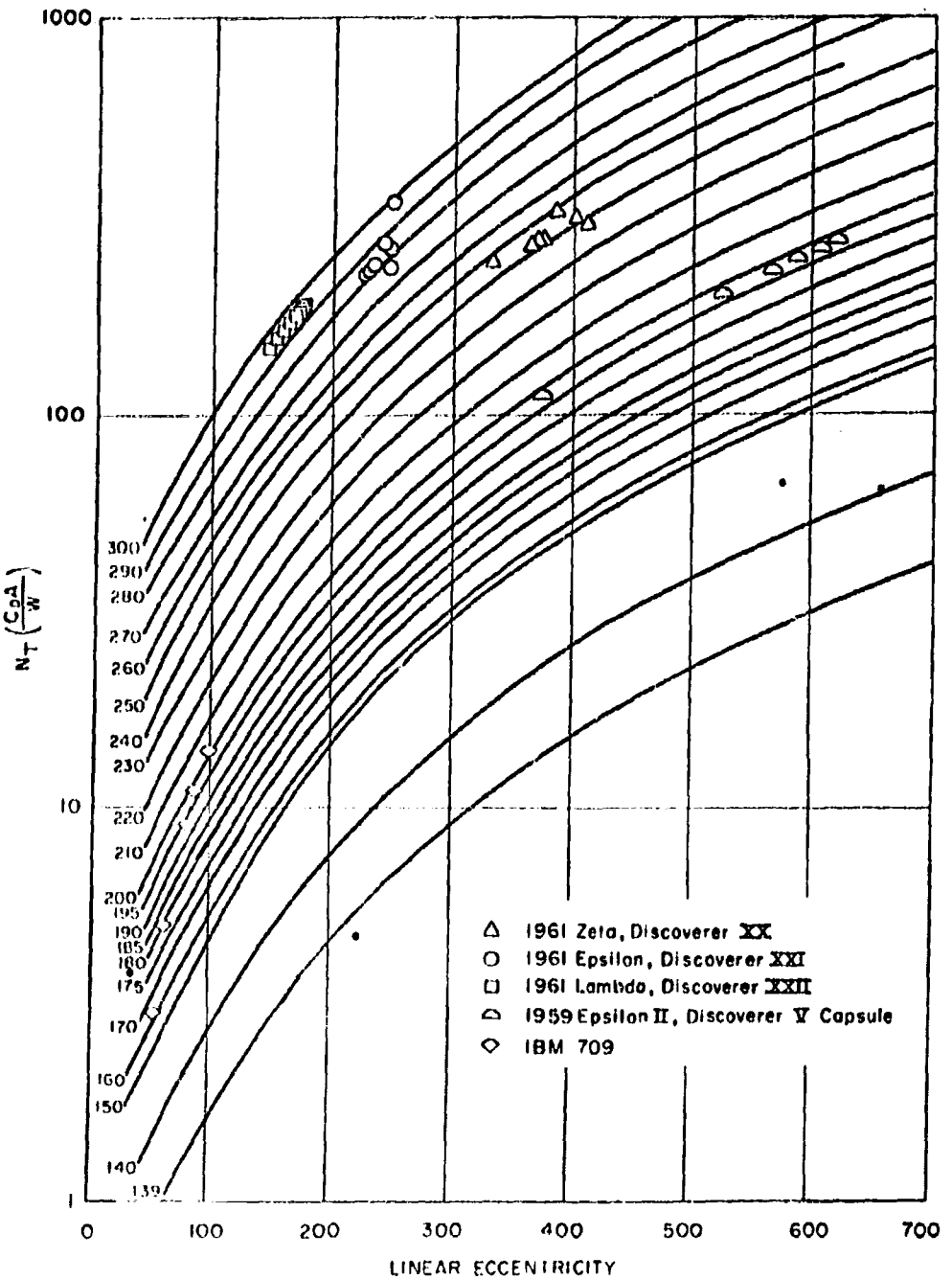

Figure 14. Comparison of observed and predicted satellite lifetime for various altitudes

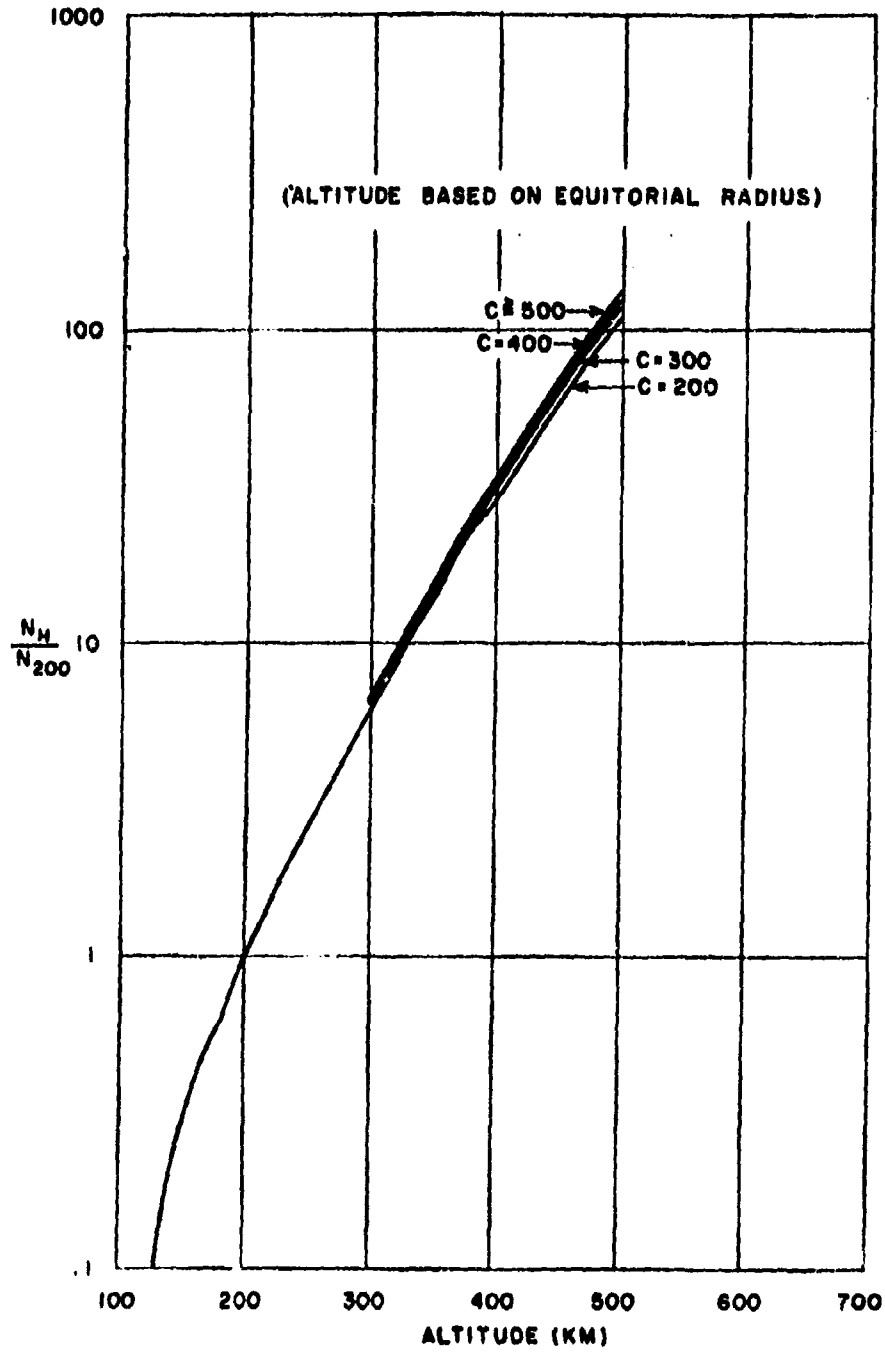

Figure 15. Normalized altitude factor

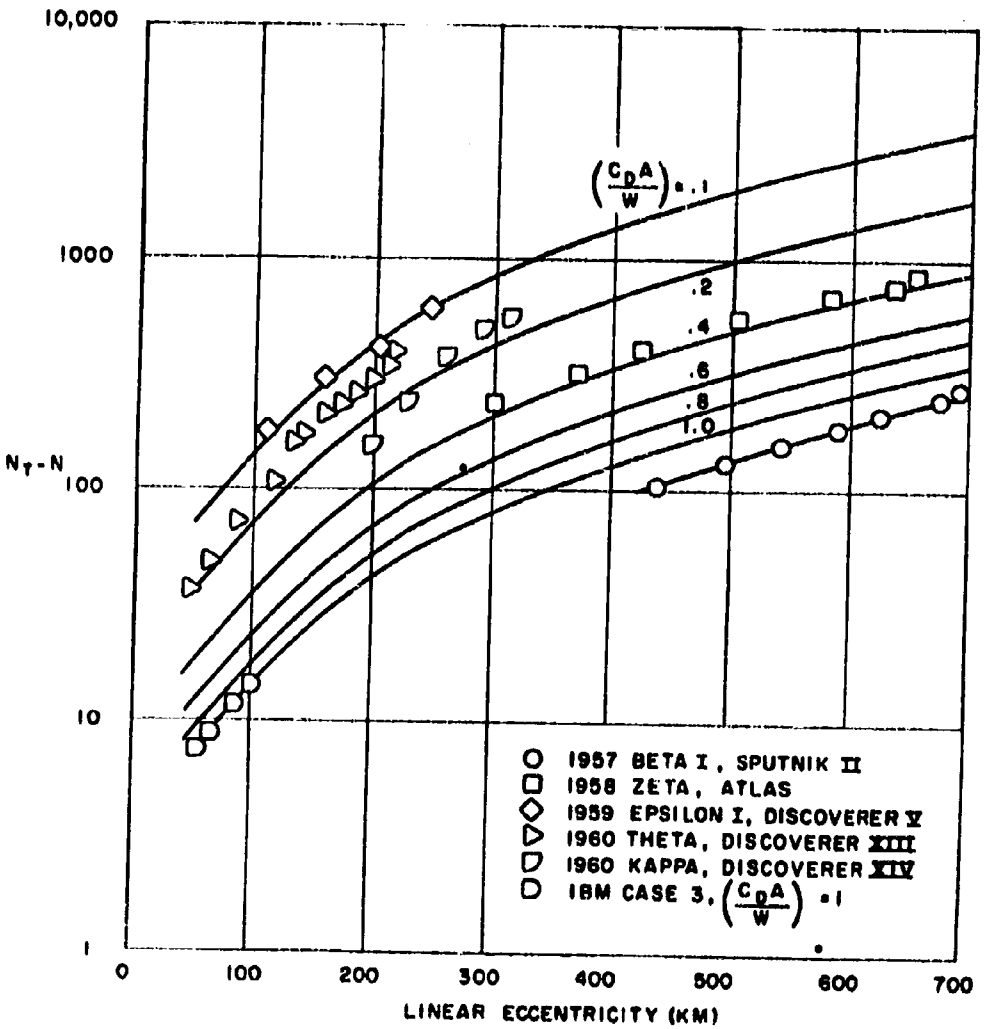

Figure 16. Comparison of observed and predicted satellite lifetime for various $C_D A/w$

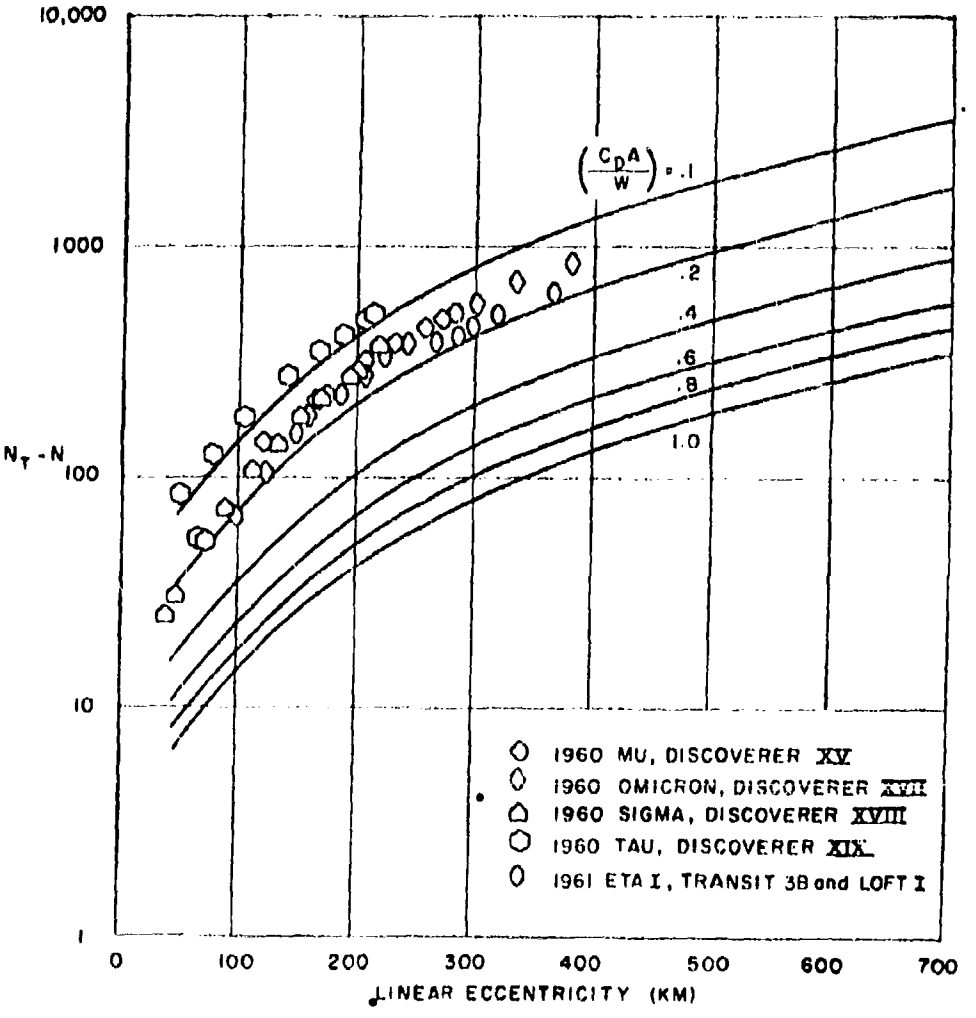

Figure 16. Concluded

Table 5-1

Ballistic Coefficients of Several Satellites

Object	Code Name	Inclination – deg	Total No. Revolutions	Ballistic Coefficient – ft^2/lb
1957 Beta	Sputnik II	65	2370	$1.25_{min} \rightarrow 1.43$
1958 Zeta	Atlas	832.3	500	0.36
1959 Epsilon I	Discoverer V	80.01	718-723	10.1
1959 Epsilon II	Discoverer V capsule	80.01	14700	0.01
1959 Zeta	Discoverer VI	84.00	965	
1960 Theta	Discoverer XIII	82.85	1498	0.143
1960 Kappa	Discoverer XIV	79.65	440	$0.125_{min} \rightarrow 0.25$
1960 Lambda II	Sputnik V rocket	64.90	563	0.06
1960 Mu	Discoverer XV	80.90	535	0.131
1960 Omicron	Discoverer XVII	81.86	720-724	0.131
1960 Sigma	Discoverer XVIII	80.82	1819	0.139
1960 Tau	Discoverer XIX	82.80	524-525	0.0868
1961 Eta	Transit 3B and Lofti	28.38	562	0.191 (variable)
1961 Zeta	Discoverer XXI	80.74	5211	0.0615

The satellites plotted in Figure 16 have inclined orbits ranging from 28 to 82 degrees. Their perigee heights range from 178 to 300 km. Even with all these wide differences, the variation of revolutions and linear eccentricity were similar and could be plotted on the same curve. Figure 16 demonstrates the close approximation of Equation (5.12) with actual satellites. The decay of 1960 Kappa appeared unique due to its marked departure from the empirical curves. The marked shift in the data from 1960 Sigma should be attributed to poor orbit information at the time of demise. The IBM program to simulate 1960 Sigma was evaluated at the wrong value of area-to-mass ratio.

VI. DISCUSSION OF SATELLITE DECAY

The purpose of this study has been to develop techniques for the analysis of satellite motion near its demise. It is well known that as the satellite approaches its demise, the usual secular motions undergo rapid changes as a result of the predominance of drag force. The approximate method developed and discussed previously, is sufficient in most cases to predict the number of revolutions before decay. This is only a gross estimate and necessarily excludes effects such as the oblate earth and a rotating atmosphere.

To explore in detail the three-dimensional motion of the satellite, the program just described has been written. It has not been possible to use this program thoroughly in an analysis and hopefully further use and analysis can be made at a later date. In the meantime a brief analysis was completed which permits a discussion of the more prominent features of the satellite motion.

The first orbit element to be studied was the linear eccentricity. This would also provide a check to the approximate solution. The rate of change of linear eccentricity per revolution with various ballistic coefficients is presented in Table 6-1. The variation of linear eccentricity for both the sphere and the cylinder were also determined assuming no heat transfer ($S_r \pm S$) and plotted in Figure 17. In Figure 17, it can be seen that the linear eccentricity decreases as expected until the satellite

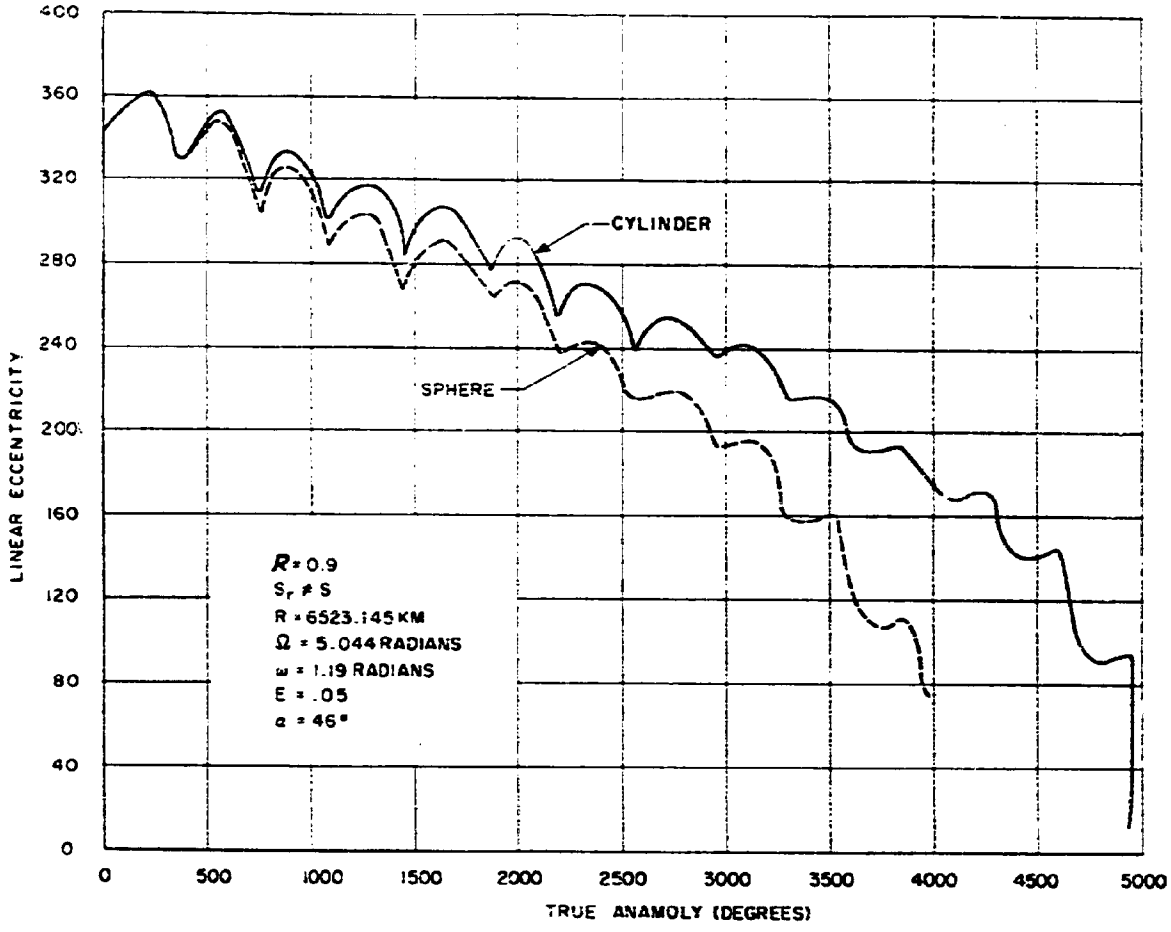

Figure 17. Decrease of linear eccentricity

descends to an altitude of 220 km, at which time, the linear eccentricity experiences short but almost instantaneous decreases.

Further study of satellite motion at very small linear eccentricity indicated poor agreement with the approximate method. Consequently, corrections were added to the approximate curves. The numerical calculations were the only means of obtaining representative satellite motion at small linear eccentricity.

Additional orbit elements were studied and are also reported in Table 6-1. The motion argument of perigee in the absence of drag can be described by Equation (3.9). At inclinations greater than 63.34 deg, the perigee moves opposite the satellite while at lower inclinations, the motion is in the direction of the satellite. For small drag forces ($D/w \leq 2.4978 \times 10^{-4}$), no effect due to drag is noticed. However, for large drag forces, radical effects are observed. A sample case is presented in Figure 18 where at about 150 km, ($D/w \approx 90$), large sudden variations in the perigee motion appear. The motion, however, remains periodic until an altitude of 110 km where the perigee then begins to travel at the rate of phi, the polar angle. It is at this same time that the emissivity has reached a maximum and begun to increase toward one. Further detail can be seen in Figures 19 and 20. These two curves are different and the difference may be due to the initial heights. Similar differences have been observed in satellite decay. For instance, the unusual behavior of 1960 Kappa as plotted in Figure 16a. The usual behavior is spiral decay at a constant perigee distance. A possible explanation for 1960 Kappa's behavio. is assuming the ballistic coefficient increased in some manner.

The eccentricity undergoes unusual changes at low altitudes. It is seen that the elliptical orbit gradually shrinks to some magic minimum, which appears also to be a function of initial conditions, and then it rapidly increases toward one as the satellite path becomes ballistic. An example of this behavior is presented in Figure 21. Table 6-2 presents some observed minimum values of eccentricity during several IBM runs.

Table 6-1
Effect of Drag on the Motion of Orbital Elements

	$\frac{C_D A}{m}$ = 0	0.01	0.1	1.0	10. $\Omega_\oplus \pm 0$	10. $\Omega_\oplus = 0$
$\frac{d\,{}_\circ\Omega_\circ}{dN}$	− 0.001392605	− 0.001391173	− 0.001391173	− 0.001391173	− 0.001391969	− 0.001392128
$\frac{dE}{dN}$	zero	9.549×10^{-8}	9.072×10^{-7}	9.135×10^{-6}	9.22×10^{-5}	1.047×10^{-4}
$\frac{d\omega}{dN}$	0.0027876	0.0027876	0.0027876	0.0027876	0.0028035	0.00281938
$\frac{di}{dN}$	1.002787	1.002787	1.002787	1.002787	1.002803	1.002819
$\frac{dR}{dN}$	zero	0.000111	0.00134	0.01351	0.1381	0.15849
$\frac{dc}{dN}$	zero	0.000677	0.0065261	0.0652642	0.6582153	0.7495464

Initial Conditions:

H = 300 km $\quad {}_\circ\Omega_{\circ_\oplus} = 7.2921 \times 10^{-5}$ rad/sec

$\phi = {}_\circ\Omega_\circ = \omega = \alpha = 0$ deg

E = 0.03

$D(m/A) = 1/2\rho V^2 \quad C_D = 2.4479$ km/sec$^2 \times 10^{-4}$

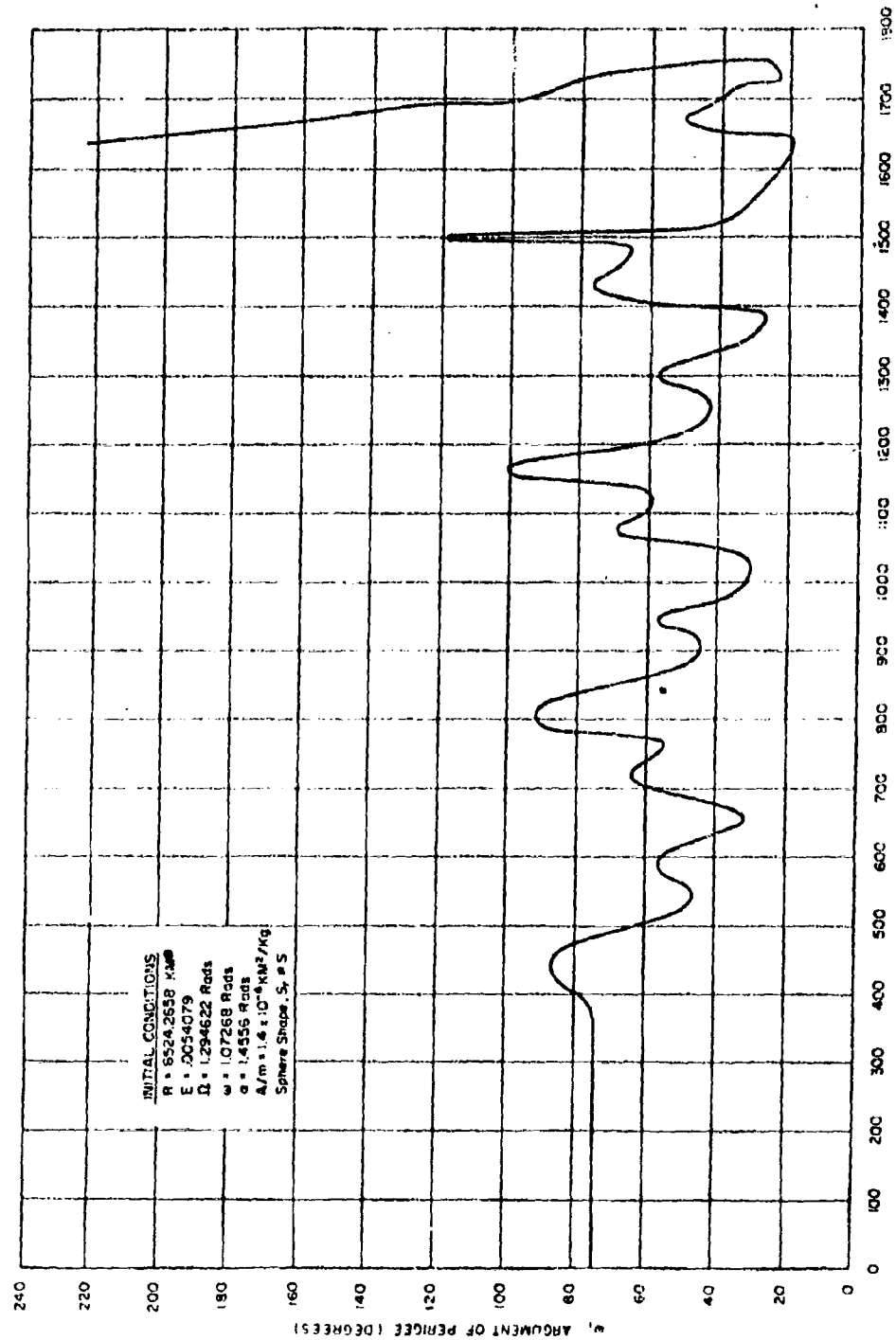

Figure 18. Motion of argument of perigee as a function of polar angle

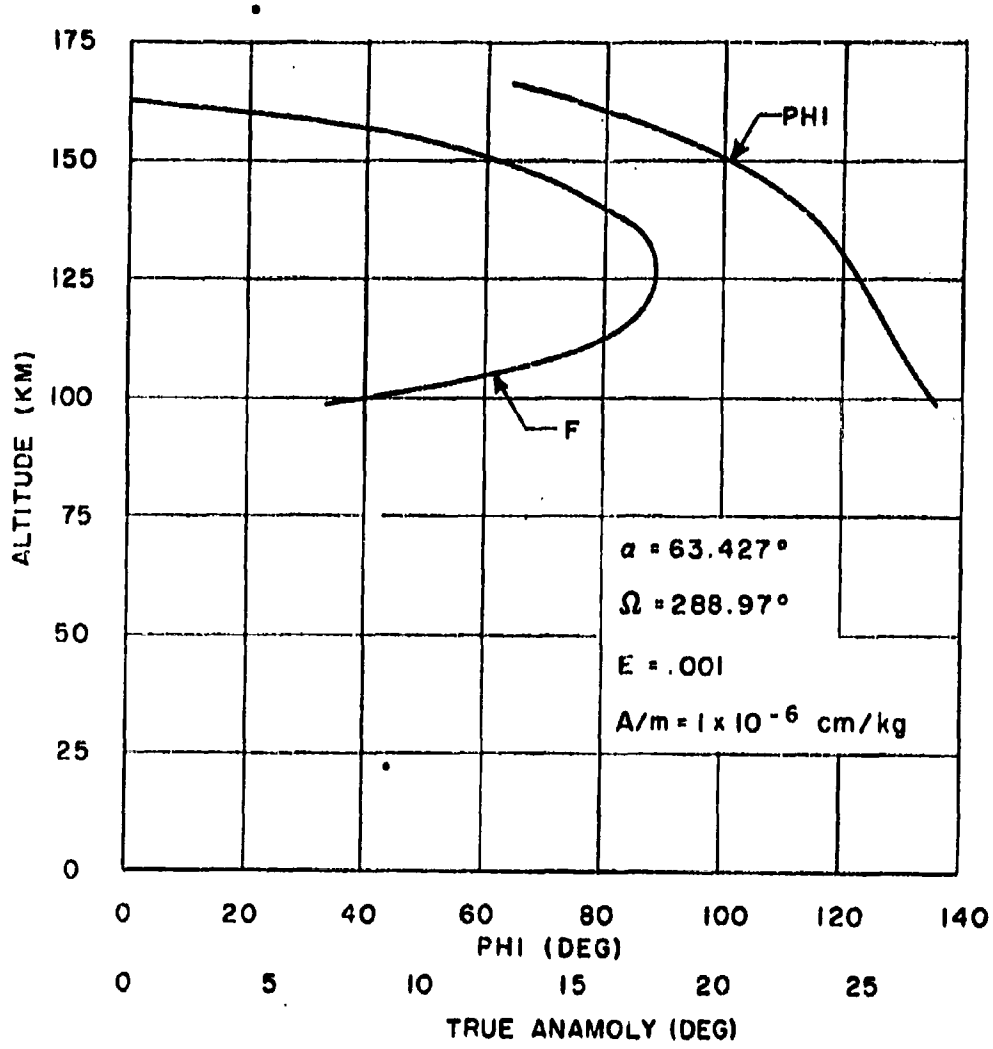

Figure 19. Motion of true anamoly at low altitudes

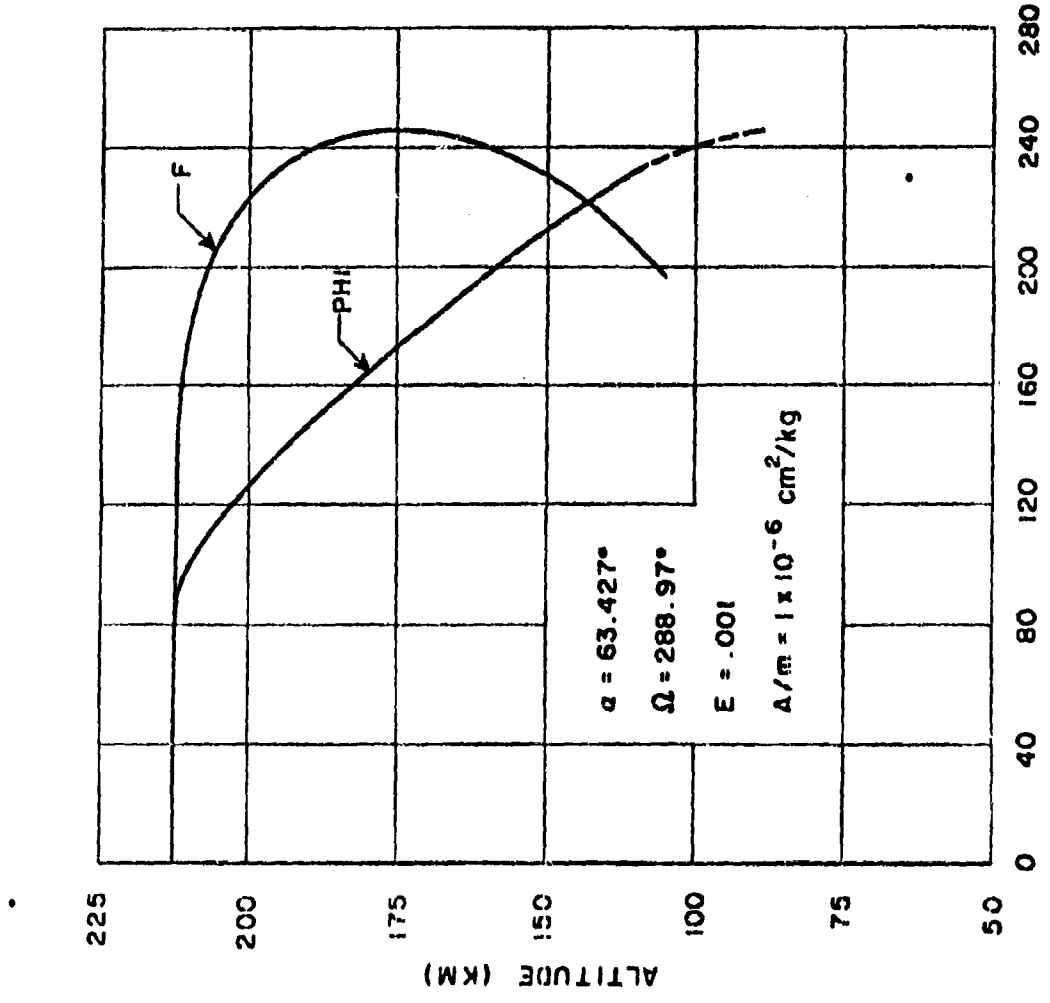

Figure 20. Motion of true anamoly at low altitudes

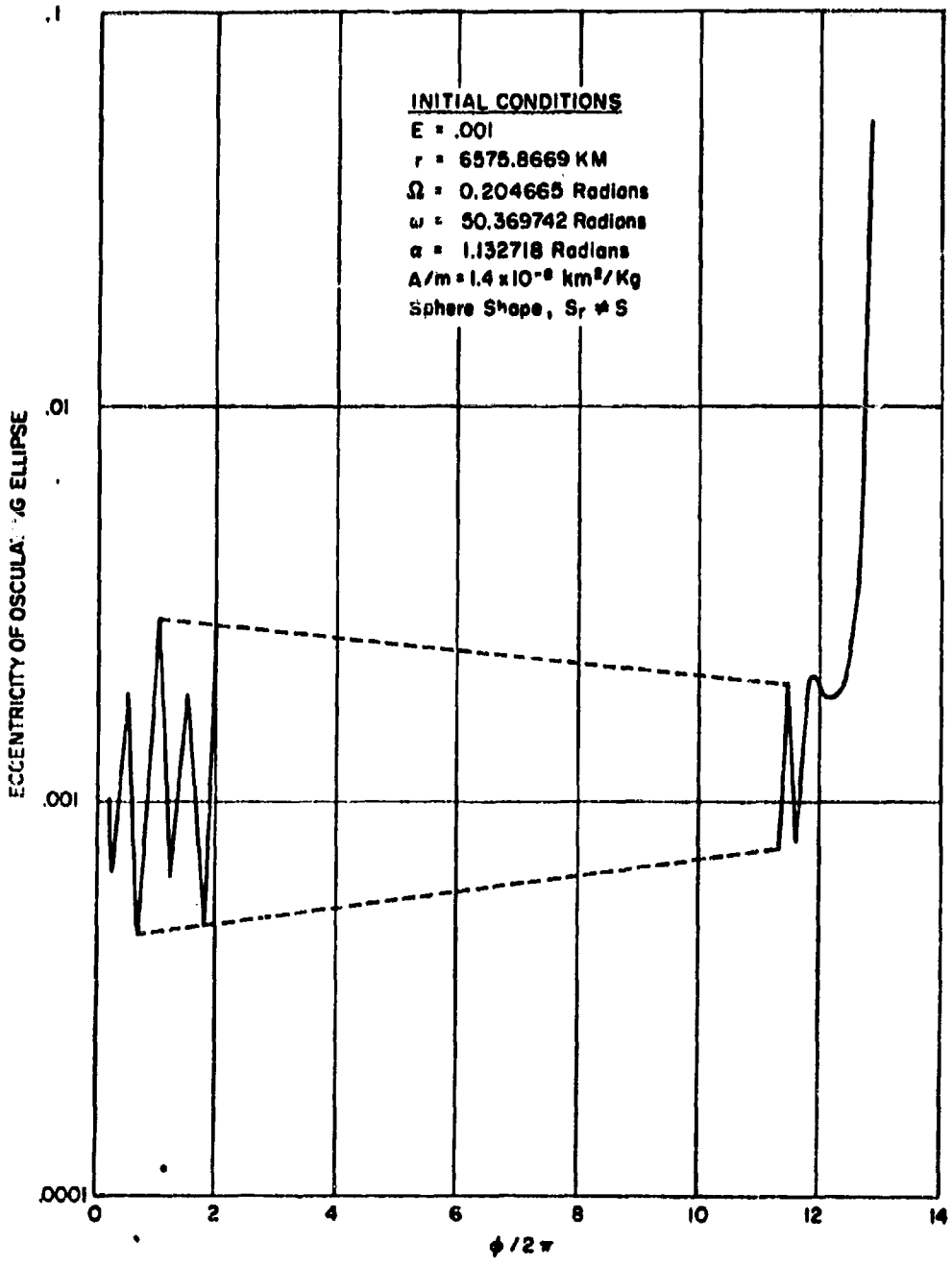

Figure 21. Variation of eccentricity at demise

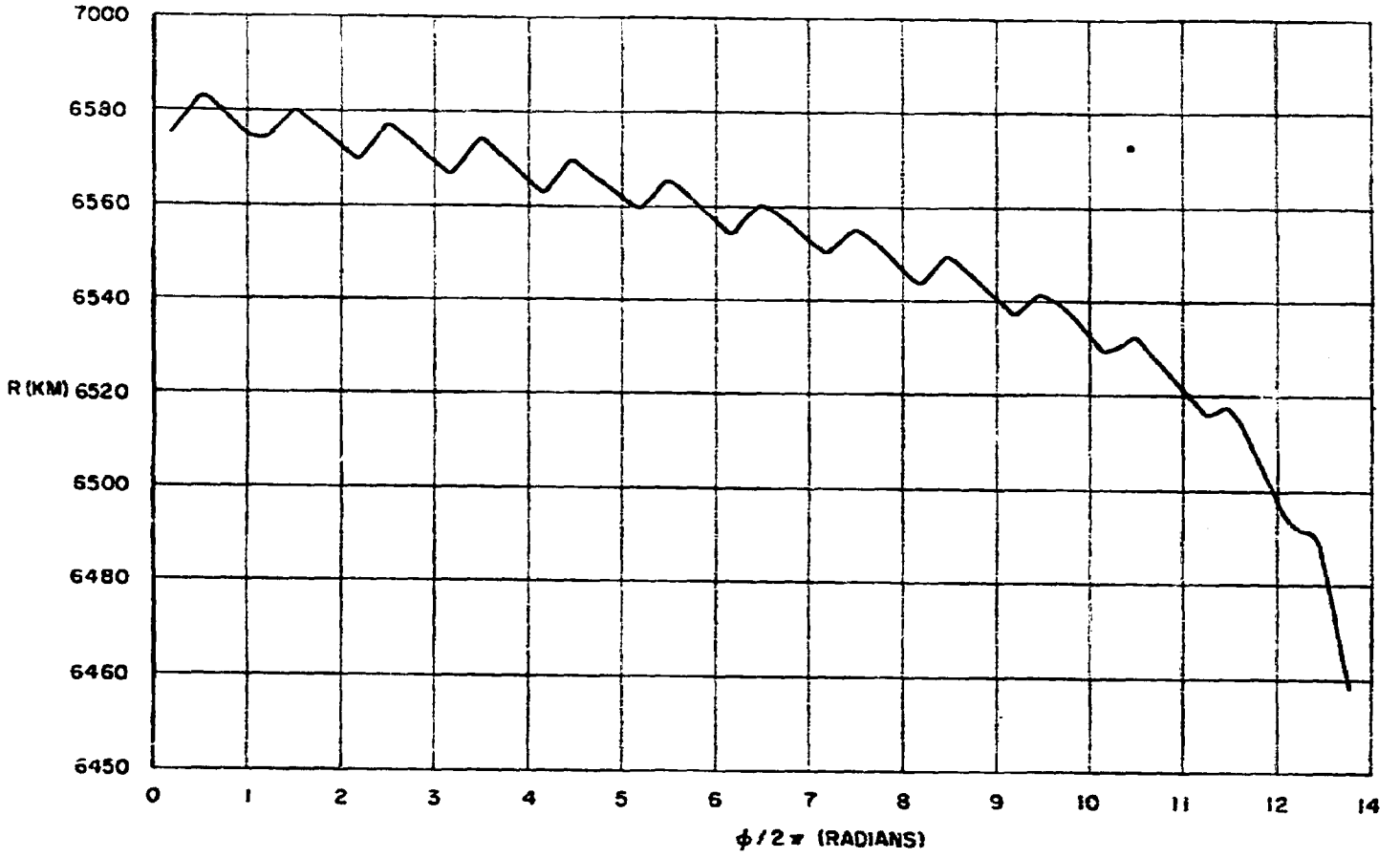

Figure 22. Decrease in perigee at demise

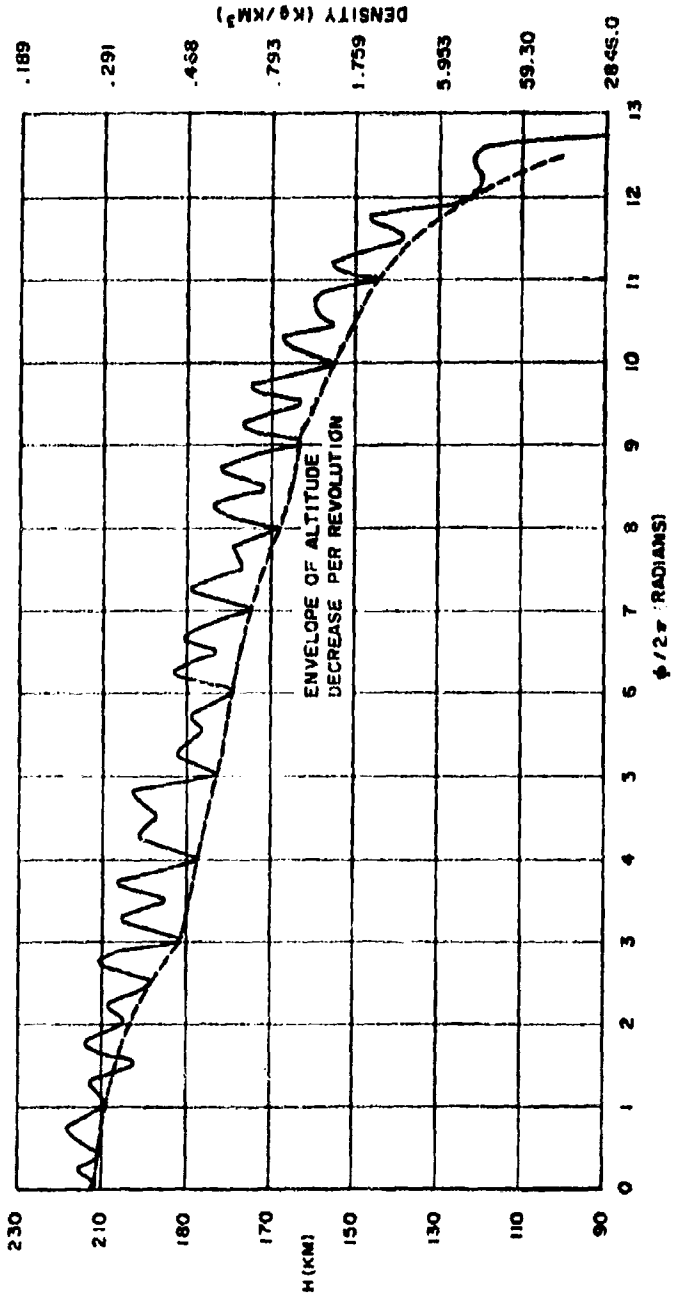

Figure 23. Variation in altitude at demise

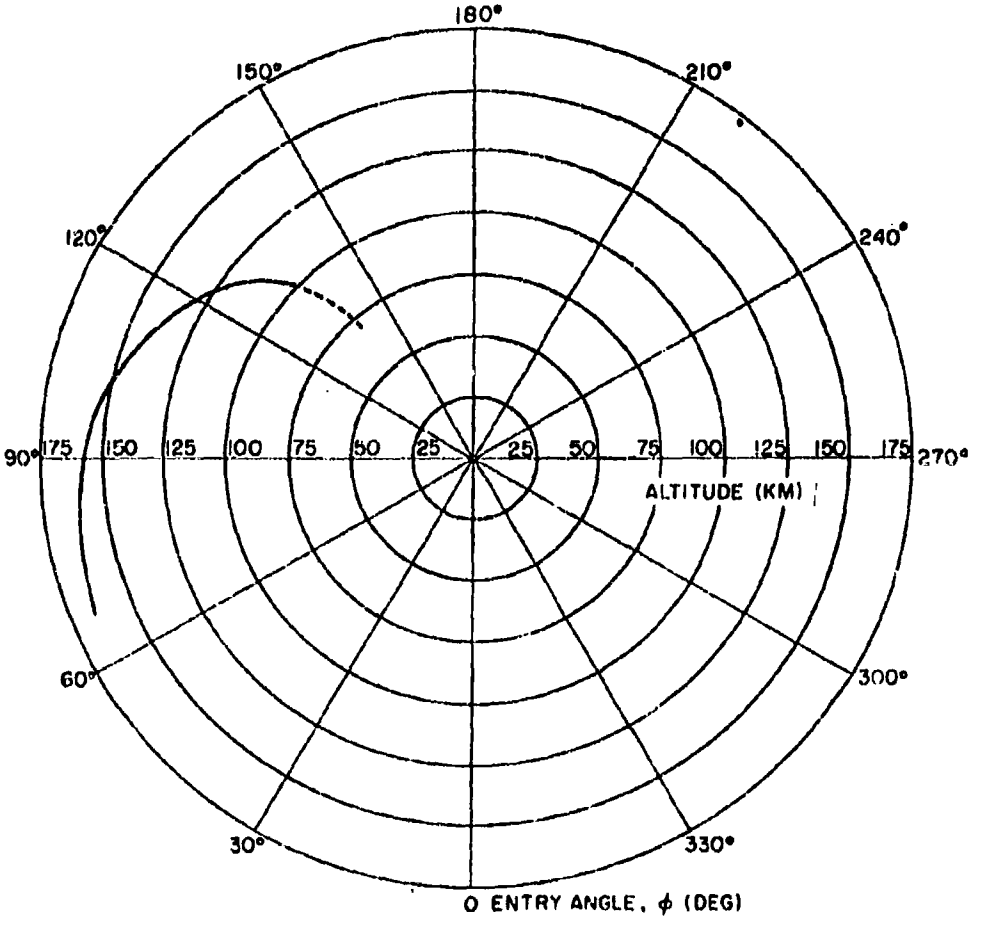

Figure 24. Satellite polar angle versus altitude

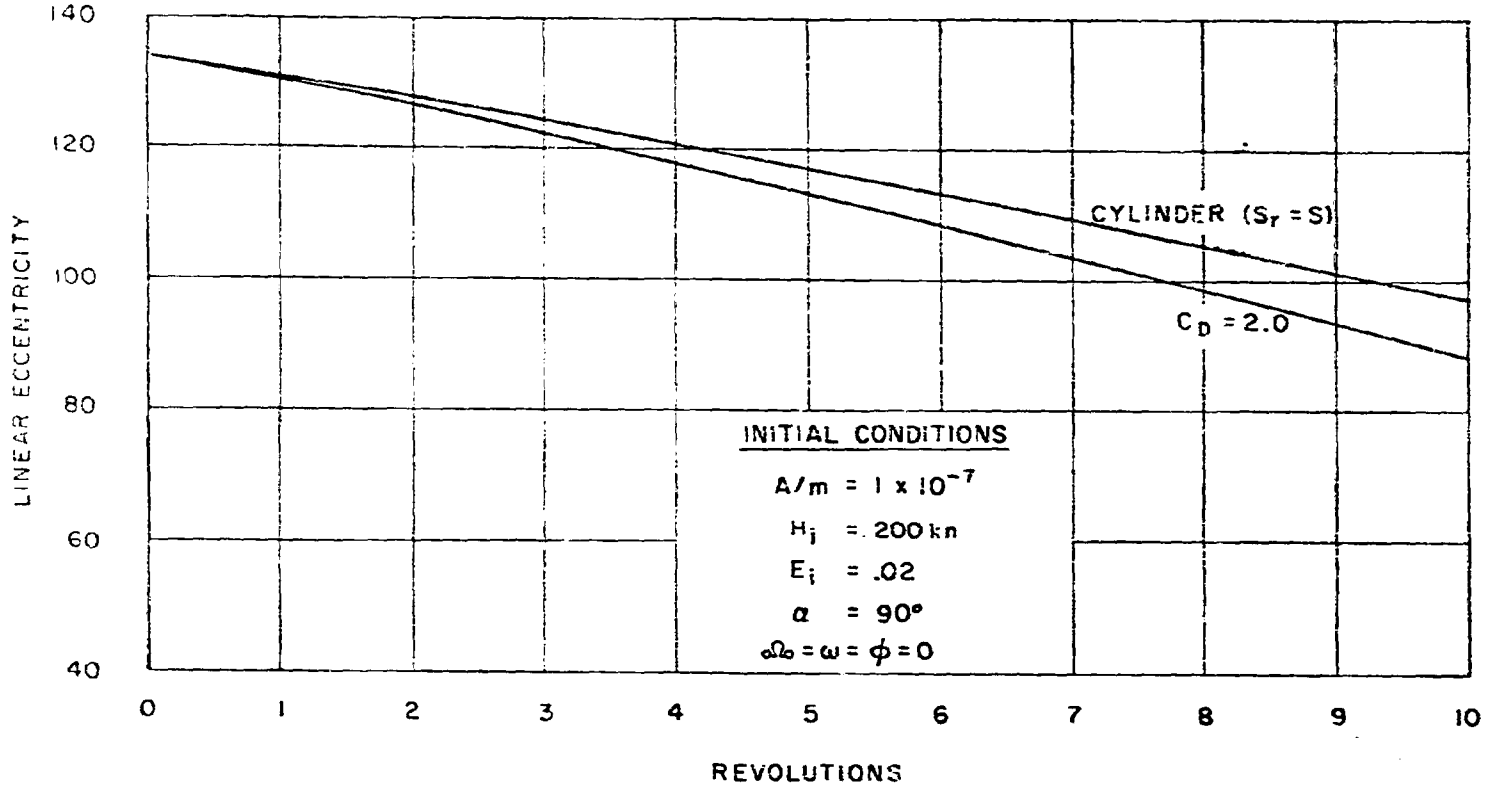

Figure 25. Error in linear eccentricity encountered by $C_D = 2.0$ as compared to cylinder

Table 6-2

Minimum Values of Eccentricity

H_i	E_i	c_i	$C_D A/w$	E_{min}	c_{min}
154	0.05	343	1.3	0.001309	8.51
194	0.0097	64.2	0.87	0.003825	21
169.8	0.00101	6.64	0.87	0.0007846	5.1
200	0.01483	99.00	1.0	0.00384	25
150	0.00761	50.054	1.0	0.003	19
200	0.00075	4.966	1.0	0.0004455	2.92615
250	0.0037576	25	1.0	0.00107	7.028
250	0.0074871	50	1.0	0.0012	8.5
140	0.044	300	1.0	0.0015	9.68
200	0.00754	50	1.0	0.0027	18.03
150	0.0151	100	1.0	0.001	9.38

The motion of the perigee and perigee altitude can be seen in Figures 22 and 23. The very unusual behavior of the perigee height is due to the earth's oblateness. Figure 24 demonstrates the rapidity of altitude loss with large drag forces. This curve is an over exaggeration of real satellites as it is based on free molecular flow even at low altitudes of 100 km. In reality, the drag coefficient is smaller than predicted by free molecular theory.

The effect of drag on the argument of right ascension is also not noticeable. With larger drag forces there is a very small increase in the backward motion of the right ascension. Even at very large forces, the change in the motion of argument of right ascension is small and nearly unnoticeable.

In all of the above computations, the atmosphere is assumed to rotate with the earth. This wind velocity when added to the satellite velocity produces an increased drag force. The enlarged drag force augments the rate of motion of all the elements. A comparison is shown in Table 6-1 between the wind on and wind off. The increase in rate in some cases is as high as ten per cent. The assumed wind velocity has not been verified and quite possibly it is too large. The assumption

becomes poorer with increasing altitude.

The initial conditions for Figures 19 through 24 are identical.

As a final comparison, the approximation often made of a constant drag coefficient equal two was compared to one computed. Figure 25 demonstrates that $C_D = 2.0$ is a poor assumption. It resulted in a loss of 0.9 km/rev linear eccentricity and a 0.3 km/rev loss in altitude over that for the computed drag coefficient using Equations (2.18) through(2.20). These are serious errors and point the need to use the more accurate representations for drag coefficient.

VII. CONCLUSIONS

A discussion of satellite motion near the end of its lifetime has been presented. The motion was observed to be very irregular under large drag forces. The effect of the irregular motion on the total satellite lifetime was small. During the time of the irregular motions, the satellite is expected to have no more than 10 to 30 revolutions remaining before decay. This is a matter of one or two days. For satellite decay predictions better than this, numerical calculations such as those used here should be employed. The program written for this study is well suited for the short range ($N \leq 500$ revolutions) predictions. Long range predictions probably require too much machine time.

Considerable effort was made to improve the approximate method. Satellite observations and numerical computations were used to adjust the approximate method. The resulting equation when used for decay predictions is accurate to three significant figures. The equation graphed is a very good way to handle the primary satellite orbit data. On the graph it is clear in what manner the satellite decays. The significance of the empirical factor $(c/100)^{0.366}$ required to correct the approximate equation has not been studied. It would be interesting to attempt to discover the effect it has on the assumption made at the beginning of the approximate method.

REFERENCES

1. Jeffrey, Harold. The Earth. Cambridge University Press, Third Edition, 1952.

2. Cornford, E. C., King-Hele, D. G., and Merson, R. H. "Recent Studies of Satellite Orbits." JAS Paper No. 59-141. Presented at the Seventh Anglo-American Aeronautical Conference, October 1959.

3. Brandeen, W. R. and Manger, W. P. "Angular Motion of the Spin Axis of the Tiros I Meteorological Satellite Due to Magnetic and Gravitational Torques." J. Geophysical Research 65, 2992 (1960).

4. Good, R. E. "A Method for Predicting the Lifetime of a Near Satellite." Massachusetts Institute of Technology, Naval Supersonic Laboratory Technical Report 418, January 1960.

5. Jacchia, Luigi G. "A Variable Atmospheric-Density Model from Satellite Accelerations." Smithsonian Institution, Astrophysical Observatory. Special Report No. 39, March 30, 1960.

6. Minzer, R. A., Champion, K. S. W., and Pond, H. L. "The ARDC Model Atmosphere, 1959." Air Force Surveys in Geophysics No. 115, AFCRC, August 1959.

7. Stalder, Jackson R., Goodwin, F. K., Creager, Marcus O. "A Comparison of Theory and Experiment for High-Speed Free-Molecule Flow." NACA Report 1032, 1951.

8. Schaaf, S. A. and Chambré, P. L. "Flow of Rarefied Gases." Fundamentals of Gas Dynamics Vol. III, High Speed Aerodynamics and Jet Propulsion. Princeton University Press, Princeton, New Jersey, 1958.

9. Stalder, Jackson R. and Zurick, Vernon J. "Theoretical Aerodynamic Characteristics of Bodies in a Free-Molecule-Flow Field." NACA TN 2423, July 1951.

10. Cook, G. E. "Aerodynamic Drag of Near Earth Satellites." RAE TN G. W. 531, September 1959. ASTIA 229535.

11. Baker, R. M. L. Jr. et al. "Efficient Precision Orbit Computation Techniques." ARS 30, 734 (August 1960).

12. _____. 704 Programmers Handbook. Share Distribution No. 602. The Ramo-Wooldridge Corp. 1958.

13. Nielsen, J. N., Goodwin, F. K., Mersman, W. A. "Three-Dimensional Orbits of Earth Satellites, Including Effects of Earth Oblateness and Atmospheric Rotation." NASA Memorandum 12-4-58a, December 1958.

14. King-Hele, D. G. and Gilmore, D. M. C. "The Effect of the Earth's Oblateness on the Orbit of a near Satellite." RAE TN No. G. W. 475, October 1957.

M.I.T. NSL TR 465 — UNCLASSIFIED

Naval Supersonic Laboratory
Massachusetts Institute of Technology
Cambridge 39, Massachusetts

A STUDY OF SATELLITE DECAY WITH THE FIRST AND SECOND ORDER GRAVITATIONAL POTENTIAL. R. E. Good. June 1961. (M.I.T. DSR 8304 - Contract AF19(604)-5894). ix and 68 pages.

The decay of earth satellites has been analyzed using both a numerical integration and an approximate method. The numerical integration utilizes the variation-of-parameter method with second order earth gravitational potential. The approximate method was developed via conservation of energy equation but for unexplained reasons would not agree with observed satellite decay without the inclusion of an additional linear eccentricity factor. Including $(c/100)^{0.366}$ permitted the approximate method to agree with numerical calculations and observed data. The usual restriction of approximate methods at low eccentricities was removed by the addition of a non-linear term previously computed numerically. The linear approximate method was found to be valid for linear eccentricities

1. Satellite decay
I. R. E. Good
II. M.I.T. NSL TR 465

UNCLASSIFIED

M.I.T. NSL TR 465 — UNCLASSIFIED

Naval Supersonic Laboratory
Massachusetts Institute of Technology
Cambridge 39, Massachusetts

A STUDY OF SATELLITE DECAY WITH THE FIRST AND SECOND ORDER GRAVITATIONAL POTENTIAL. R. E. Good. June 1961. (M.I.T. DSR 8304 - Contract AF19(604)-5894). ix and 68 pages.

The decay of earth satellites has been analyzed using both a numerical integration and an approximate method. The numerical integration utilizes the variation-of-parameter method with second order earth gravitational potential. The approximate method was developed via conservation of energy equation but for unexplained reasons would not agree with observed satellite decay without the inclusion of an additional linear eccentricity factor. Including $(c/100)^{0.366}$ permitted the approximate method to agree with numerical calculations and observed data. The usual restriction of approximate methods at low eccentricities was removed by the addition of a non-linear term previously computed numerically. The linear approximate method was found to be valid for linear eccentricities

1. Satellite decay
I. R. E. Good
II. M.I.T. NSL TR 465

UNCLASSIFIED

M.I.T. NSL TR 465 — UNCLASSIFIED

Naval Supersonic Laboratory
Massachusetts Institute of Technology
Cambridge 39, Massachusetts

A STUDY OF SATELLITE DECAY WITH THE FIRST AND SECOND ORDER GRAVITATIONAL POTENTIAL. R. E. Good. June 1961. (M.I.T. DSR 8304 - Contract AF19(604)-5894). ix and 68 pages.

The decay of earth satellites has been analyzed using both a numerical integration and an approximate method. The numerical integration utilizes the variation-of-parameter method with second order earth gravitational potential. The approximate method was developed via conservation of energy equation but for unexplained reasons would not agree with observed satellite decay without the inclusion of an additional linear eccentricity factor. Including $(c/100)^{0.366}$ permitted the approximate method to agree with numerical calculations and observed data. The usual restriction of approximate methods at low eccentricities was removed by the addition of a non-linear term previously computed numerically. The linear approximate method was found to be valid for linear eccentricities

1. Satellite decay
I. R. E. Good
II. M.I.T. NSL TR 465

UNCLASSIFIED

M.I.T. NSL TR 465 — UNCLASSIFIED

Naval Supersonic Laboratory
Massachusetts Institute of Technology
Cambridge 39, Massachusetts

A STUDY OF SATELLITE DECAY WITH THE FIRST AND SECOND ORDER GRAVITATIONAL POTENTIAL. R. E. Good. June 1961. (M.I.T. DSR 8304 - Contract AF19(604)-5894). ix and 68 pages.

The decay of earth satellites has been analyzed using both a numerical integration and an approximate method. The numerical integration utilizes the variation-of-parameter method with second order earth gravitational potential. The approximate method was developed via conservation of energy equation but for unexplained reasons would not agree with observed satellite decay without the inclusion of an additional linear eccentricity factor. Including $(c/100)^{0.366}$ permitted the approximate method to agree with numerical calculations and observed data. The usual restriction of approximate methods at low eccentricities was removed by the addition of a non-linear term previously computed numerically. The linear approximate method was found to be valid for linear eccentricities

1. Satellite decay
I. R. E. Good
II. M.I.T. NSL TR 465

UNCLASSIFIED

larger than 150. The effect of a variable drag coefficient and projected area was found to be an important factor and of the order e^2.

larger than 150. The effect of a variable drag coefficient and projected area was found to be an important factor and of the order e^2.

larger than 150. The effect of a variable drag coefficient and projected area was found to be an important factor and of the order e^2.

larger than 150. The effect of a variable drag coefficient and projected area was found to be an important factor and of the order e^2.